



This is a repository copy of *Structural behaviour and design of end-restrained square tubed-reinforced-concrete columns exposed to fire.*

White Rose Research Online URL for this paper:  
<https://eprints.whiterose.ac.uk/173035/>

Version: Accepted Version

---

**Article:**

Yang, D., Liu, F., Huang, S.-S. [orcid.org/0000-0003-2816-7104](https://orcid.org/0000-0003-2816-7104) et al. (1 more author) (2021) Structural behaviour and design of end-restrained square tubed-reinforced-concrete columns exposed to fire. *Journal of Constructional Steel Research*, 182. 106675. ISSN 0143-974X

<https://doi.org/10.1016/j.jcsr.2021.106675>

---

© 2021 Elsevier. This is an author produced version of a paper subsequently published in *Journal of Constructional Steel Research*. Uploaded in accordance with the publisher's self-archiving policy. Article available under the terms of the CC-BY-NC-ND licence (<https://creativecommons.org/licenses/by-nc-nd/4.0/>).

**Reuse**

This article is distributed under the terms of the Creative Commons Attribution-NonCommercial-NoDerivs (CC BY-NC-ND) licence. This licence only allows you to download this work and share it with others as long as you credit the authors, but you can't change the article in any way or use it commercially. More information and the full terms of the licence here: <https://creativecommons.org/licenses/>

**Takedown**

If you consider content in White Rose Research Online to be in breach of UK law, please notify us by emailing [eprints@whiterose.ac.uk](mailto:eprints@whiterose.ac.uk) including the URL of the record and the reason for the withdrawal request.



[eprints@whiterose.ac.uk](mailto:eprints@whiterose.ac.uk)  
<https://eprints.whiterose.ac.uk/>

# Structural behaviour and design of end-restrained square tubed-reinforced-concrete columns exposed to fire

Dongdong Yang <sup>a,b</sup>, Faqi Liu <sup>a,b,\*</sup>, Shan-Shan Huang <sup>c</sup>, Hua Yang <sup>a,b</sup>

<sup>a</sup> *Key Lab of Structures Dynamic Behaviour and Control (Harbin Institute of Technology), Ministry of Education, Heilongjiang, Harbin 150090, China*

<sup>b</sup> *Key Lab of Smart Prevention and Mitigation of Civil Engineering Disasters (Harbin Institute of Technology), Ministry of Industry and Information Technology, Heilongjiang, Harbin 150090, China*

<sup>c</sup> *Department of Civil and Structural Engineering, The University of Sheffield, Sir Frederick Mappin Building, Mappin Street, Sheffield S1 3JD, UK*

## Abstract

Tubed-reinforced-concrete columns are gaining increasing usage in engineering practices, whereas research on their fire behaviour is still limited and mainly concentrated on unrestrained columns. Since end-restrained columns might behave differently in fire as compared to the unrestrained columns, the fire behaviour of square tubed-reinforced-concrete columns with end restraints was investigated via numerical modelling in this study. The axial and rotational restraints were modelled using linear springs and then validated against fire test results. The effects of end restraints on the failure mode, axial force and buckling length at failure and fire resistance, and on the evolution of deformations, internal force and bending moment during heating, of end-restrained columns were systematically analysed through parametric studies. The axially-restrained columns mostly undergo axial contraction only in fire; their typical failure mode is uncontrolled overall axial deformation, except for those columns of relatively high axial restraints. An increase in axial restraint leads to a nearly linear decrease of axial force at failure and a linear increase of fire resistance. For rotationally-restrained columns, the typical failure mode is also uncontrolled overall axial deformation. As the rotational restraint increases, the buckling length at failure decreases and

the fire resistance increases, which is particularly significant when the rotational restraint is relatively low. A practical design method is proposed for the fire resistance design of square tubed-reinforced-concrete columns with either axial, or rotational, or combined axial and rotational restraints. Both constant and temperature-dependent end restraints have been adopted and the outcome is that they provide very similar results.

**Keywords:** Square tubed-reinforced-concrete column; Axial restraints; Rotational restraints; Fire resistance; Finite element modelling; Structural fire design.

\* Corresponding author, E-mail address: [fqliu@hit.edu.cn](mailto:fqliu@hit.edu.cn)

## 1. Introduction

Tubed-reinforced-concrete (TRC) column, also named as steel tube confined reinforced concrete (STCRC) column, is a new type of steel-concrete composite column, in which the reinforced concrete (RC) section is confined by a steel tube. The steel tube of a TRC column is cut at the column-beam connections, and so the steel tube mainly provides confinement to the inner RC and does not sustain the axial load directly, as shown in Fig. 1. These cutting gaps also allow the release of the vapour from the concrete core subject to heating. Compared to the concrete-filled steel tubular (CFST) columns whose steel tube and concrete core sustains the axial load together, much thinner steel tubes are generally used in TRC columns since the local buckling of the steel tube can effectively be minimised. For the purpose of resisting bending effects and enhancing the fire resistance, reinforcing bars are essential in TRC columns. Owing to the high bearing capacity, good ductility, excellent seismic performance and ease of construction, TRC columns are increasingly used in construction practices, especially in China [1]. Over the past decades, extensive research has been carried out on the behaviour of square and circular TRC columns at ambient temperatures [2-8]. The Chinese national standard JGJ/T471 [9] provides the design guidance of TRC columns.

Although structural fire safety is one of the key design considerations of columns, the research on the fire behaviour of TRC columns is still limited. Liu et al. [10] have investigated the fire behaviour of circular TRC columns, both experimentally and

numerically, and they have proposed a practical fire design method. Additional fire tests of five square and two rectangular slender TRC columns have been reported by the authors of this paper [11, 12]. A finite element analysis (FEA) model has also been developed and validated against experiments [12]. Then the model has been used for comprehensive parametric studies, facilitating the development of the fire design method for the square and rectangular TRC columns [12].

However, all the studies on TRC columns discussed above are associated with isolated members without considering the effects of column end restraints. In a building fire, when the fire exposure is affecting the main height of the column, the adjoining structures may remain relatively cool and act as end restraints to the heated member. Within non-sway frames, such restraints can generally consist of axial and rotational constraints of deformations, as shown in Fig. 2. The restraint degrees at column ends may vary depending on the engineering practice and the existence of end restraints is believed to affect the axial and rotational deformation behaviour of the heated column, thus having inevitable impact on the internal stress resultants and the fire resistance of the column. However, the fire behaviour of end-restrained square TRC columns has never before been reported in detail, motivating the work presented in this paper.

Over the past four decades, the performance of end-restrained steel columns at high temperatures has been extensively studied [13-24] and relevant research on CFST columns and steel columns encased in concrete has also been widely reported [25-34]. Rotational restraint will have a favourable influence on the fire resistance of steel and steel-concrete composite columns, since the rotational restraint reduces the buckling length compared to the equivalent case of unrestrained columns. The influence of axial restraint on the fire behaviour of steel and steel-concrete composite columns is complicated. On one hand, the restrained axial thermal elongation imposes additional axial force inside the column during the initial heating and is thus detrimental. On the other hand, when the column starts to contract as temperature rises, the axial restraint becomes beneficial as it relieves the axial force in the column. Since the previous studies [11, 12] indicate that the working mechanism of TRC columns exposed to fire is very different from those of the steel columns, CFST

columns and steel columns encased in concrete, it is expected that the effects of end restraints on the fire performance of TRC columns may also be different from those of the other column types referred to above.

In the present research, the fire performance of axially-loaded restrained square TRC columns in non-sway frames has been studied using the FEA modelling. The restraints at column ends have been taken into account investigating systematically the effects of axial and rotational restraints on the overall deformations, internal axial forces and bending moments, failure modes and fire resistance of square TRC columns. The key parameters studied in the FEA modelling include cross-sectional dimensions, slenderness ratio, load ratio and restraint ratio of the column. A structural fire safety design method for end-restrained square TRC columns with either axial, or rotational, or combined axial and rotational restraints has been thereby proposed, introducing also the effects of the temperature-dependent end restraints on the fire behaviour of the columns.

## **2. Description and validation of the FEA modelling**

### *2.1 Setup of the model*

The sequentially-coupled thermo-mechanical ABAQUS model that was developed and validated for unrestrained TRC columns in the authors' previous study [11, 12] has further been developed to model the restrained square TRC columns in this study. The temperature-dependent specific heat and thermal conductivity proposed by Lie [35] and recommended by ASCE [36] for concrete with carbonate aggregate and steel are used in the thermal analysis. The mechanical analysis adopts the compressive stress-strain relationship of concrete proposed by Lie [35], the tensile constitutive model of concrete developed by Hong and Varma [37] and the high-temperature stress-strain models of structural steel and rebars given in Eurocodes [38, 39]. Other details of this FEA model, e.g. the interaction and constraint, element types and meshing, can be found in references [11, 12] and are not repeated here. Since there is no clear definition of the failure of restrained TRC columns, the failure criteria used for unrestrained TRC columns are again adopted. In this way, the fire resistance of the

column is defined as the time when the axial deformation exceeds  $L/100$  or when the deformation rate reaches  $3L/1000$  mm/min, where  $L$  is the length of the column in mm [40]. Since the focus of this study is on the TRC columns in braced or non-sway frames, the lateral deformations at the column ends are restricted. Due to the geometry and loading symmetries, only half of the column cross-section is modelled, as shown in Fig. 3. The top and bottom ends of the RC section are set as rigid bodies, whose DoFs are those of the corresponding reference points RP1 and RP2. These two reference points are connected to spring elements (Spring1). The rotational restraints at the top and bottom ends of the column are simulated by two rotational springs. Only the top end of the column is restrained axially, modelled by an axial spring. The rotational restraints are assumed identical at both ends of the column. The end restraints are assumed to remain unchanged during heating, since only the TRC column is exposed to fire.

The restraint level at the column end is quantitatively represented by the ratio between the stiffness provided by the surrounding structures and the stiffness of the column itself. The normalized axial restraint ratio  $\alpha$  and rotational restraint ratio  $\beta$  at ambient temperatures are defined as,

$$\alpha = k_a/k_{ac} \quad (1)$$

$$\beta = k_r/k_{rc} \quad (2)$$

where  $k_a$  and  $k_r$  are the axial and rotational restraint stiffnesses provided by the surrounding structures at ambient temperatures, respectively;

$k_{ac}$  and  $k_{rc}$  are the axial and rotational stiffnesses of the TRC column at ambient temperatures, respectively;

$$k_{ac} = (E_c A_c + E_b A_b)/L;$$

$$k_{rc} = 4(E_c I_c + E_b I_b + E_s I_s)/L;$$

$E_c$  is the tangent modulus of the concrete;

$E_b$  and  $E_s$  are the elastic moduli of the reinforcing bars and the steel tube, respectively;

$A_c$  and  $A_b$  are the cross-sectional areas of the concrete and the reinforcing bars, respectively;

$I_c$ ,  $I_b$  and  $I_s$  are the second moments of area of the concrete, the rebars and the steel tube with respect to the centroidal axis of the composite cross-section, respectively.

## 2.2 Validation against CFST tests

As mentioned in Section 2.1, the FEA model has already been validated against fire tests [11, 12], including 11 TRC and 90 CFST columns with square, rectangular or circular cross-sections, filled with plain or bar-reinforced concrete, with or without fire protection and with pinned-pinned, fixed-fixed or pinned-fixed boundary conditions. The model has been extended to consider the end restraints of TRC columns and so the modelling of the column-end restraints using spring elements has been validated in this study. Fire tests of TRC columns with non-ideal end restraints have not been reported so far and therefore the high-temperature tests by Pires et al. [28] and Rodrigues and Laim [29, 30] on 34 full-scale CFST columns (six square specimens, six rectangular specimens and 22 circular specimens) considering realistic end restraints are employed for the validation. These end-restrained CFST specimens have been provided by either axial or axial and rotational restraints. The details of the tests are summarised in Table 1. In the tests, the axial and rotational restraints provided by the surrounding structures to the heated CFST column have been simulated by a 3D restraining steel frame, creating different restraint levels by varying the frame span, as illustrated in Fig. 4 taken from the reference [29]. The restraint level remained unchanged during a test until failure.

Spring elements of restraint stiffnesses, identical to those measured during the tests of references [28-30] are adopted in the FEA modelling. The measured furnace temperature-time curves are used in the heat transfer analysis. The predicted cross-section temperature-time relationships, axial deformation-time relationships and relative axial restraining force ( $P/P_0$ )-time relationships of some example restrained CFST columns are compared with the test results in Figs. 5-7. The critical time and the ratio between the maximum axial compression force inside the column and the initial applied load predicted by the FEA for all these 34 end-restrained columns are compared with the test results in Table 1. A good agreement between the experimental and numerical results has generally been achieved, indicating that the model is capable of predicting the fire behaviour of steel-concrete composite columns with end restraints. Thereby the model is used as the basis to evaluate the influence of end restraints on the fire behaviour of square TRC columns in this study.

### 2.3 Comparison with frame modelling

The effectiveness of simplifying the restraints at the column ends using springs in the FEA model is further assessed in this section using a 2D frame model, as shown in Fig. 8. The size of the square cross-section is 600 mm and the slenderness ratio of the column is 30. The applied load induces a load ratio of 0.5. The column bottom end is either ideally fixed or pinned and two rectangular RC beams are connected to the column top. The cross-section size of the beam is 300 mm  $\times$  500 mm with a nominal reinforcement ratio of 1.5%. The effective length to sectional depth ratio of the RC beam is 12 and the beam is fixed at the end not connected to the column. According to Eqs. (1) and (2), the axial and rotational restraint ratios provided by these two beams are 0.006 and 0.419, respectively.

The development of the axial deformation at the column top end, the lateral deformation at the column mid-height and the axial force at the column bottom end, as well as the lateral deformations and bending moments along the column length at failure, are illustrated in Fig. 8. The difference between the spring and frame models is insignificant, indicating that the spring model can be used as a simplified alternative to simulate the frame restraints. The buckling length  $L_{\text{eff}}$  of the TRC column exposed to fire corresponds to the distance between the bending moment zero points, as shown in Fig. 2. The ratio between  $L_{\text{eff}}$  and the whole length of the column  $L$  is defined as the buckling length ratio  $\mu_f$ . For columns with the bottom end fixed or pinned,  $\mu_f$  is 0.566 or 0.703, respectively, as determined by the bending moment diagrams shown in Fig. 8(e).

To isolate the effects of the axial and rotational restraints, six different boundary conditions at the top end of the column are assessed in the FEA, i.e. (i) frame, (ii) axial and rotational springs, (iii) only axial spring and free to rotate, (iv) only rotational spring and free to move axially, (v) pinned but free to move axially and (vi) fixed to rotate and free to move axially. Fig. 9 shows the axial deformation-time relationships resulting from these six different boundary conditions. Before reaching the failure, the differences between these cases are negligible. However, compared to Case (v), the end restraints result in an obvious delay of the column failure. The fire resistances of Cases (iii) and (iv) lie in between those of Cases (v) and (vi). The enhancement of the column fire resistance caused by the rotational restraint

(Case (iv)) is more apparent than that of the axial restraint (Case (iii)). It is interesting to note that the column in the frame model (Case (i)) reaches an even longer fire resistance than Case (vi), which is particularly apparent in Fig. 9(b). This might reflect the effect of the axial restraint on the fire resistance, which applies to Case (i) but not to Case (vi).

### 3. Effect of axial restraint

#### 3.1 Parametric studies

The axial restraint ratio  $\alpha$  of a circular CFST column in a CFST column-steel beam frame is within the range of 0.005 to 0.1 [33] and the range of  $\alpha$  of a RC column in a RC frame is 0.005 to 0.15 [41].

Square TRC columns are usually connected to rectangular RC beams to form composite frames. The axial restraint level  $\alpha$  of a TRC column is directly affected by various factors, such as the location of the heated column (interior or exterior), the number of the storeys of the frame (single or multiple), the frame type (plane or 3D) and the dimensions of the columns and beams. On the basis of structural mechanics, the axial restraint stiffness  $k_a$  of the following three simple cases are calculated and given as:

(a) For a column in a single-storey frame:

$$k_a = \sum_{i=1}^{m_{ba}} k_{bai} \quad (3)$$

(b) For a ground-floor column in a two-storey frame:

$$k_a = \sum_{i=1}^{m_{ba}} k_{bai} + \frac{1}{\frac{1}{k_{ca}} + \frac{1}{\sum_{i=1}^{m_{ba}} k_{bai}}} \quad (4)$$

(c) For a ground-floor column in a three-storey frame:

$$k_a = \sum_{i=1}^{m_{ba}} k_{bai} + \frac{\frac{1}{k_{ca}} + \frac{2}{\sum_{i=1}^{m_{ba}} k_{bai}}}{\frac{1}{k_{ca}^2} + \frac{3}{k_{ca} \cdot \sum_{i=1}^{m_{ba}} k_{bai}} + \frac{1}{\sum_{i=1}^{m_{ba}} k_{bai} \cdot \sum_{i=1}^{m_{ba}} k_{bai}}} \quad (5)$$

where  $k_{bai}$  is the rotational stiffness provided by the RC beam  $i$ ;

$k_{bai} = 12(EI)_{bi}/L_{bi}^3$ , where  $(EI)_{bi}$  is the flexural stiffness and  $L_{bi}$  is the effective length of the RC beam  $i$ ;

$m_{ba}$  is the number of the beams connected to the heated column;

$k_{ca}$  is the axial stiffness of the unheated column directly above the heated one;

$k_{ca} = (EA)_c/L_c$ , where  $(EA)_c$  is the axial stiffness and  $L_c$  is the effective length of the unheated column.

Eq. (6) is recommended by Shepherd [17] for determining the axial restraint ratio  $\alpha_m$  of a ground column in a multi-storey frame with  $m$  storeys. This equation is valid when all the storeys of the frame have identical beam framing and all the beams are of identical dimensions. To achieve a more accurate prediction, the equation considers also the axial deformability of the columns above the heated one.

$$\alpha_m = f_{\alpha_1}(\alpha_{m-1}) = \alpha_1 + \frac{1}{1 + \frac{1}{\alpha_{m-1}}} \quad (6)$$

where  $\alpha_{m-1}$  is the axial restraint ratio of the ground column in the frame with  $m-1$  storeys and  $\alpha_1$  corresponds to an identical column in a single-storey frame.

The evolution of the  $\alpha_m - \alpha_1$  relationship as the number of the storeys  $m$  increases is shown in Fig. 10. When the frame is higher than 10 storeys, the number of the storeys has almost

no influence on the total axial restraint ratio and  $\alpha_m$  converges to  $\frac{\alpha_1 + \sqrt{\alpha_1^2 + 4\alpha_1}}{2}$ . According

to Eq. (6), as well as the Chinese design codes JGJ/T471 [9], JGJ 3 [42] and GB 50010 [43], the range of  $\alpha$  for a square TRC column in a frame of TRC columns and RC beams is approximated as 0.005 to 0.1.

The influences of various parameters, such as the axial restraint ratio  $\alpha$  (0.01 to 0.1), load ratio  $n$  (0.3 to 0.7), sectional size  $D$  (200 to 1500 mm) and slenderness ratio  $\lambda$  (30 to 60) on

the fire behaviour of axially-restrained square TRC columns are discussed in this section. For the unrestrained TRC columns,  $\alpha$  is equal to zero. The cylinder strength of the concrete,  $f'_c$  is 40 MPa, the yield strength of the steel tube,  $f_y$  is 345 MPa and the yield strength of the rebars,  $f_b$  is 355 MPa. The sectional steel area ratio  $\alpha_s$  (the ratio between the area of the steel tube and the area of the concrete) is 3% and the reinforcement ratio  $\rho$  (the ratio between the area of the reinforcing bars and the area of the concrete) is 4%. The columns are heated following the ISO 834 standard fire [40] along the whole length.

### 3.2 Results and discussion

Fig. 11 presents a typical example for the effects of axial restraint on the axial deformation, lateral deformation, axial force at the top end, spring force and bending moment at the mid-height of the column for a TRC column with  $D = 200$  mm,  $\lambda = 30$  and  $n = 0.5$ . The positive notation in Fig. 11(a) is for expansion and negative is for contraction. It is found that all the modelled columns experience axial contraction only during the entire heating period. As the restraint ratio  $\alpha$  increases, both the axial compressive deformation and its rate decrease, indicating the positive effect of the axial restraint on the fire performance of the column. As shown in Figs. 11(c) and 11(d), as the compressive deformation of the column increases, the axial spring is in tension and the axial force transferred into the column decreases. The higher the axial restraint ratio, the larger the spring force and the lower the axial force in the column. All the columns with no axial restraint ( $\alpha = 0$ ) or with low or medium axial restraints ( $\alpha < 0.1$  in this case) fail when the increase of axial deformation becomes uncontrollable. When the axial restraint is extremely high ( $\alpha = 0.1$  in this example), this failure mode is avoided. Figs. 11(b) and 11(e) show that the increase of axial restraint also leads to the decrease of lateral deformation and bending moment at the mid-height of the column.

Fig. 12 presents the axial deformation vs. time relationships for the TRC columns of 200 mm size, corresponding to various axial restraint ratios (0 to 0.1), load ratios (0.3 to 0.7) and slenderness ratios (30 and 50). Obvious axial expansion is observed only in the columns subject to the smallest load ratio 0.3. All the other columns experience only contraction during the entire heating process. As shown in Figs. 12(a) and 12(c), the axial deformations

of columns with different axial restraints reverse from expansion to contraction at almost the same temperature. Similar behaviour has been reported in previous research [17, 28, 31] on the fire behaviour of end-restrained steel and CFST columns. When the reversal in the direction of the axial deformation occurs, the thermal expansion counteracts fully the axial contraction induced by the loading of the superstructure and material degradations at high temperatures. At this point, the restraint force is zero. This might explain why the deformation reversal temperatures of the cases with different restraints are very similar. However, more research is required to confirm this.

For axially restrained steel columns, CFST columns and steel columns encased in concrete exposed to fire, most researchers [13, 23, 30, 32] define the failure taking place when the axial compressive force in the column becomes identical with the initial applied load, or when the axial deformation of the column is identical to the deformation under ambient-temperature loading, since the column is considered not being able to withstand the initial applied serviceability load afterwards. However, the definition of the failure in the restrained columns exposed to fire is a very complex issue [19] and there is no agreement on it within the current structural fire design codes worldwide. Even though the axial force of the column is lower than the initial applied load, the whole frame could still perform effectively as long as the unheated adjacent members connected to the heated column do not fail. Therefore, the above failure criteria may be conservative for axially restrained columns. On the other hand, these criteria are not applicable to columns that do not experience apparent axial elongation at elevated temperatures. As found in this study (Figs. 11 and 12) and in previous research [11, 12], most of the square TRC columns with common load ratios (larger than 0.3) undergo no or very modest axial elongation in fire. Therefore, it is decided not to adopt the above-mentioned failure criteria, but to apply the failure criteria for unrestrained columns given in ISO 834 [40] to the restrained TRC columns dealt with in this study.

The relationships between the fire resistance and axial restraint ratio of axially restrained TRC columns with different dimensions, load ratios and slenderness ratios are shown in Fig. 13. The fire resistance generally increases linearly with the increase in the axial restraint ratio. This beneficial effect of the axial restraint ratio is more apparent in the relatively stocky

columns than in the relatively slender columns. This is because for achieving the same axial restraint ratio, the end restraint stiffness values applied to slenderer columns must be lower than those applied to stockier ones. To give an example, the end stiffness of the TRC column with a slenderness ratio of 30 is nearly twice of that in the column with a slenderness ratio of 50. The effect of axial restraint is more complex in columns subject to relatively low load ratios. Since those columns tend to experience axial expansion during the initial heating, the axial restraint will cause additional compression and increase the axial force in the column, potentially decreasing the fire resistance. As the column gets into the contraction stage during the temperature rise, the effect of the axial restraint turns beneficial, since it actually results in a continual decrease of the axial force in the column.

Fig. 13(h) illustrates the comparison between the fire resistance of axially-restrained and unrestrained columns. The average of the ratios between the fire resistances of the axially-restrained columns and those of the unrestrained columns (the slopes of the dash lines in Fig. 13(h)) increases linearly from 1.11 to 1.62 as the restraint ratio increases from 0.01 to 0.05. As described in Section 2.3, in the single storey frame with TRC columns and RC beams shown in Fig. 8, the square TRC column with  $D = 600$  mm and  $\lambda = 30$  has an axial restraint ratio  $\alpha_1$  of approx. 0.006 and the enhancement factor for the fire resistance caused by the axial restraint is only approx. 0.06. However, as the number of storeys in the frame increases to 10, the enhancement in the fire resistance may be greater than 70%, since the axial restraint ratio  $\alpha_{10}$  calculated using Eq. (6) becomes 0.06. This beneficial effect of axial restraint is relatively significant and should not be ignored in engineering design.

### *3.3 Proposed design method*

Due to the axial restraint, the axial force within the TRC column changes continuously during heating. To quantify the influence of the axial restraint on the fire resistance of the column, the axial force ratio at failure  $n_f$  is introduced, indicating the ratio of the axial force at failure in the heated column to the buckling resistance of the column at ambient temperatures. The axial force ratios  $n_f$  at failure obtained from the FEA are plotted against the axial restraint ratios  $\alpha$  in Fig. 14. In general,  $n_f$  decreases linearly with the increase of  $\alpha$ . This trend is much

larger for relatively stocky columns (i.e.  $\lambda = 30$ ) than for relatively slender columns ( $\lambda = 50$ ), which is consistent with the results in Fig. 13.

A simplified regression formula, Eq. (7), is proposed for determining the relationship between  $n_f$  and  $\alpha$ ,

$$n_f = n - (3.6 - 0.047\lambda) \cdot \alpha \quad (7)$$

Fig. 15(a) shows a good agreement between the  $n_f$  values calculated using Eq. (7) and those obtained from the FEA.

During heating, the buckling resistance of a column decreases due to material weakening. At the same time, the axial force in the column also decreases as part of the applied load is carried by the axial spring. The column fails when the buckling resistance of the heated column falls below its axial force, and the time for this is the fire resistance. The authors have proposed a practical design method [12] for predicting the buckling resistance  $N_{b,T}$  for the square TRC columns exposed to fire, as shown in Eqs. (8)-(29).

$$N_{b,T} = \varphi_T N_{u,T} \quad (8)$$

$$N_{u,T} = (f_{c,eq,T} + 5.1 f_{el,T}) A_c + f_{b,T} A_b \quad (9)$$

$$f_{c,eq,T} = \beta_{cT} k_{cT} f_c' \quad (10)$$

$$\beta_{cT} = \frac{1}{1 + (0.0054t + 0.22) \sqrt{\frac{t}{D_c}}} \quad (11)$$

$$k_{cT} = 1 - \left( \frac{0.045}{D_c} - 0.016 \right) t \quad (12)$$

$$f_{el,T} = \frac{1.5 k_{s,T} t_s f_{y,T}}{D} \quad (13)$$

$$k_{s,T} = \frac{27 t_s}{D} \sqrt{\frac{f_{y,T}}{235} \left( \frac{30}{f_{c,eq,T}} \right)} \quad (14)$$

$$f_{y,T} = k_{yT} f_y \quad (15)$$

$$k_{yT} = \begin{cases} 1 & 0.02 \leq T_{sn} \leq 0.4 \\ 44.55 T_{sn}^5 - 186.48 T_{sn}^4 + 301.96 T_{sn}^3 - 232.73 T_{sn}^2 + 82.52 T_{sn} - 9.78 & 0.4 < T_{sn} \leq 1.1 \\ -0.2 T_{sn} + 0.24 & 1.1 < T_{sn} \leq 1.2 \end{cases} \quad (16)$$

$$T_s = 1080 - 450 \exp(-0.8t) - 630 \exp(-3t) + 20 \quad (17)$$

$$f_{b,T} = k_{bT} f_b \quad (18)$$

$$k_{bT} = \begin{cases} 1 & 0.02 \leq T_{bn} \leq 0.4 \\ 44.55T_{bn}^5 - 186.48T_{bn}^4 + 301.96T_{bn}^3 - 232.73T_{bn}^2 + 82.52T_{bn} - 9.78 & 0.4 < T_{bn} \leq 1.1 \\ -0.2T_{bn} + 0.24 & 1.1 < T_{bn} \leq 1.2 \end{cases} \quad (19)$$

$$T_b = (T_s - 20) \exp \left\{ \left( \frac{13.5(2x/D_c - 1)}{(0.36t/D_c^2)^{3/4}} \right) \left( 1 - 1.5 \left( \frac{2y}{D_c} \right)^2 \left( 1 - \frac{2x}{D_c} \right) \right) \right\} + 20 \quad (20)$$

$$\varphi_T = \frac{1}{\Phi + \sqrt{\Phi^2 - \bar{\lambda}_T^2}} \quad (\text{EC3}) \quad \text{or}$$

$$\varphi_T = \begin{cases} 1 & \bar{\lambda}_T \leq 0.15 \\ \left[ 1 + (1 + \varepsilon_1) / \bar{\lambda}_T^2 \right] / 2 - \sqrt{\left[ 1 + (1 + \varepsilon_1) / \bar{\lambda}_T^2 \right]^2 / 4 - 1 / \bar{\lambda}_T^2} & 0.15 \leq \bar{\lambda}_T \leq 1 \quad (\text{JGJ/T471}) \\ \left[ 1 + (1 + \varepsilon_2) / \bar{\lambda}_T^2 \right] / 2 - \sqrt{\left[ 1 + (1 + \varepsilon_2) / \bar{\lambda}_T^2 \right]^2 / 4 - 1 / \bar{\lambda}_T^2} & \bar{\lambda}_T \geq 1 \end{cases} \quad (21)$$

$$\bar{\lambda}_T = \sqrt{\frac{N_{u,T}}{N_{cr,T}}} \quad (22)$$

$$N_{cr,T} = \frac{\pi^2 (EI)_{fi,eff}}{L_{eff}^2} \quad (23)$$

$$(EI)_{fi,eff} = k_{sET} E_s I_s + k_{bET} E_b I_b + C k_{cET} E_c I_c \quad (24)$$

$$k_{sET} = \begin{cases} 1 & 0.02 \leq T_{sn} \leq 0.1 \\ -T_{sn} + 1.1 & 0.1 < T_{sn} \leq 0.5 \\ 7.62T_{sn}^4 - 31.17T_{sn}^3 + 47.38T_{sn}^2 - 31.93T_{sn} + 8.14 & 0.5 < T_{sn} \leq 1.2 \end{cases} \quad (25)$$

$$k_{bET} = \begin{cases} 1 & 0.02 \leq T_{bn} \leq 0.1 \\ -T_{bn} + 1.1 & 0.1 < T_{bn} \leq 0.5 \\ 7.62T_{bn}^4 - 31.17T_{bn}^3 + 47.38T_{bn}^2 - 31.93T_{bn} + 8.14 & 0.5 < T_{bn} \leq 1.2 \end{cases} \quad (26)$$

$$C = 0.6 + 2 \frac{\alpha_s + \rho}{1 + \alpha_s + \rho} \leq 0.9 \quad (27)$$

$$k_{cET} = k_{cFT} \cdot \frac{2636}{2500 + \left[ 6 \cdot \left( \frac{-9.8t^2 + 92.7t}{D_c} + 20 \right) + 0.04 \cdot \left( \frac{-9.8t^2 + 92.7t}{D_c} + 20 \right)^2 \right]} \quad (28)$$

$$L_{eff} = \mu_f L \quad (29)$$

Here  $t$  is the duration of heating in hours according to ISO 834 standard fire curve [40];

$D_c$  is the cross-section width of the concrete core in metres;

$D$  is the outer width of the steel tube in metres;

$t_s$  is the wall thickness of the steel tube in metres;

$x$  and  $y$  are the distances from the rebar location to the symmetry axes of the cross-section in metres;

Eq. (16), Eq. (19), Eq. (25) and Eq. (26) are based on the tabulated values given in EC4 [44];

$$T_{sn} = T_s/1000;$$

$$T_{bn} = T_b/1000;$$

$\varphi_T$  ( $\varphi_T \leq 1$ ) is the buckling reduction coefficient which is based on the buckling curves given in Clause 6.3.1.2 of EC3 [45] or the buckling curve of square TRC columns given in JGJ/T471 [9], as well as the relative slenderness of the column at elevated temperatures  $\bar{\lambda}_T$ .

In EC3 [45],  $\Phi$  is a parameter used for the determination of the reduction coefficient  $\varphi_T$ .  $\Phi = 0.5[1 + \alpha_{imp}(\bar{\lambda}_T - 0.2) + \bar{\lambda}_T^2]$ , where  $\alpha_{imp}$  is the imperfection factor corresponding to the appropriate buckling curve;

$\varepsilon_1$  and  $\varepsilon_2$  are the equivalent imperfection factors given in JGJ/T471 [9], related to the cross-section type. For square TRC columns,  $\varepsilon_1 = 0.499\bar{\lambda}_T - 0.074$  and  $\varepsilon_2 = 1.461\bar{\lambda}_T - 1.036$ .

Fig. 15(b) presents the comparison between the high-temperature buckling resistance determined using Eq. (8) for the failure time evaluated on account of the FEA and the axial force at failure calculated using Eq. (7) for the columns dealt with in the parametric studies above. The agreement is reasonable, indicating that the design method of Eq. (8) proposed in reference [12] together with the axial force ratio at failure of Eq. (7) can be used to evaluate the fire resistance for the axially restrained square TRC columns.

## 4. Effect of rotational restraint

### 4.1 Parametric studies

For a column in a one-storey frame or on the top floor of a multi-storey frame, the rotational restraint stiffness  $k_r$  at the top end of the column equals to  $\sum_{i=1}^{m_{br}} k_{bri}$ , where  $m_{br}$  is the number of the beams connected to the column in direction of either its major or minor axis of bending,

whichever is of interest. For a corner column,  $m_{br} = 1$  and for other cases,  $m_{br} = 2$ .  $k_{bri}$  is the rotational stiffness provided by the beam  $i$  and  $k_{bri} = 4(EI)_{bi}/L_{bi}$ .

For the columns at other locations,  $k_r = \sum_{i=1}^{m_{br}} k_{bri} + k_{cr}$ , where  $k_{cr}$  is the rotational stiffness of the upper column that adjoins the heated column;  $k_{cr} = 4(EI)_c/L_c$ , where  $(EI)_c$  is the flexural stiffness of the upper column.

Wang et al. [34] found that the rotational restraint ratio  $\beta$  for CFST columns is between 0 and 4, and a constant value of 2 was used by Wu and Qiao [41] for RC columns. A preliminary estimate indicates that  $\beta = 0$  to 5 is applicable to most of the square TRC columns used in engineering practices in China. This section presents parametric studies on the influence of rotational restraint on the fire behaviour of square TRC columns. Parameters investigated include rotational restraint ratio  $\beta$  (0 to 5), load ratio  $n$  (0.4 to 0.7), sectional size  $D$  (200 to 1500 mm) and slenderness ratio  $\lambda$  (30 to 60). Three ideal boundary conditions, both ends pinned (PP), both ends fixed (FF) and one end pinned and another end fixed (PF) are also included in the parametric studies to enable comparisons. It should be noted that the load ratio and slenderness ratio are calculated based on the PP boundary conditions and they are not calculated again when the boundary conditions vary.

## 4.2 Results and discussion

Figs. 16(a) to 16(g) present the results from the FEA modelling for a typical TRC column ( $D = 200$  mm,  $\lambda = 30$  and  $n = 0.5$ ), including the axial deformation, the maximum lateral deformation and top end rotation in the column, restraining moment in the spring, bending moment at the mid-height of the column, the distribution of lateral deformation along the column length and the distribution of bending moment along the column length at the moment of failure. Similar axial deformation behaviour is found for the analysed TRC columns restrained rotationally with different restraint ratios. All these columns fail due to the uncontrolled increase of axial deformations. When the rotational restraint increases, the column end rotation and mid-height lateral deformation both decrease significantly, as shown in Figs. 16(b) and 16(c). The bending moment  $M_m$  at the column mid-height is the sum of the

second-order moment  $M_\delta$  and the spring restraining moment  $M_r$ , as illustrated in Fig. 17. The rotational restraint ratio  $\beta$  may affect simultaneously both  $M_\delta$  and  $M_r$ .  $M_\delta$  increases as the lateral deformation at the column mid-height increases. Therefore, an increase in  $\beta$ , which decreases the lateral deformation of the column, will cause a decrease in  $M_\delta$ . Since  $M_r$  is the spring rotation multiplied by the spring stiffness, the influence of rotational restraint on  $M_r$  is not monotonous. When the rotational restraint is relatively low (e.g.  $\beta < 0.05$  in Fig. 16),  $M_r$  increases with the increasing rotational restraint. For columns with relatively high rotational restraint (e.g.  $\beta > 0.05$  in Fig. 16), an increase in rotational restraint results in a decrease of  $M_r$ . Since  $M_\delta$  is larger than  $M_r$  in the cases analysed, an increase of  $\beta$  leads to a decrease in  $M_m$  and an enhancement of the column fire resistance, as shown in Fig. 16(e). As expected, the end rotations at failure in the columns with higher rotational restraints are smaller than those in the columns with lower rotational restraints, as shown in Fig. 16(f). The column mid-height bending moment at failure decreases with the increase of restraining level, as shown in Fig. 16(g).

Fig. 16(h) presents the buckling length ratios  $\mu_f$  at failure for the columns ( $D = 200$  mm,  $\lambda = 30$ ,  $n = 0.5$ ) with different rotational restraint ratios, together with the fire resistance of the column  $t_{FR}$ . As the rotational restraint ratio increases from 0 to 5, the fire resistance of the column increases from 79.9 min to 127.5 min and the buckling length ratio at failure decreases simultaneously from 1 to 0.5. This beneficial effect of rotational restraint is particularly obvious when  $\beta$  is within the range of 0 to 0.5. The column with PF boundary condition has a fire resistance of 108.5 min, which is equivalent to that of the column with a rotational restraint ratio of 0.026, based on linear interpolation. The fire performance of the column with  $\beta \geq 5$  appears to be almost the same as that of the column with FF boundary conditions.

Although the ambient-temperature stiffness of the heated column is used to define the restraint level in Section 2.1, the flexural stiffness of the column actually degrades during heating due to the degradation of the mechanical properties at high temperatures, causing the real-time rotational restraint ratio to increase. This results in the decrease of the buckling length as temperature increases, as shown in Fig. 16(i). When  $\beta$  is within the range of 0.01

to 0.05, this descending trend of buckling length is particularly obvious. For example, the buckling length ratio in the column with  $\beta = 0.05$  decreases from 0.9 (before heating) to 0.6 (at failure) after heating.

The influence of the rotational restraint on the fire resistance of the column is shown in Fig. 18, as the comparison for the columns with PF and FF boundary conditions. Consistent with the conclusions drawn from Fig. 16(h), the increase of rotational restraint ratio leads to an obvious increase in the fire resistance of the column, especially when  $\beta$  is between 0 to 0.5 for the columns considered in this study. In general, relatively large rotational restraints (i.e.  $\beta > 5$  for the columns analysed in this study) could lead to nearly the same fire resistance as for the case with FF boundary conditions. The rotational restraint ratio, equivalent to the PF boundary condition, is generally around 0.02 to 0.04 for TRC columns with a slenderness ratio of 30. It ranges between 0.05 to 0.1 when the slenderness ratio of the column is 50.

Fig. 18 also shows that the ratios between the fire resistances of the columns with and without rotational restraints increase as the load ratio or slenderness increases. This might be because: 1) the fire resistance of the unrestrained column is low when the load ratio or slenderness is relatively high; 2) an increase in the load ratio or slenderness may result in an increase in the end rotation of the column and thus increase the reduction of the bending moment in the mid-height of the column, enhancing the fire resistance further.

### *4.3 Proposed design method*

Most of the current structural fire design methods for steel-concrete composite columns, such as those given in the European code EC4 [44] and Chinese code GB 50936 [46], have focused mainly on pin-ended columns. EC4 provides a rough guide on the buckling lengths of the heat-affected CFST columns in braced frames, considering the effect of boundary conditions. If each of the frame storeys is considered as a fire compartment with sufficient fire resistance, the buckling length may be taken as  $0.5L$  for a column on an intermediate storey and as  $0.7L$  for a column on the top floor. For a heated column on the lowest floor, the buckling length depends on the rotational rigidity of the column base and may vary from  $0.5L$  to  $0.7L$ . However, the buckling length of a column exposed to fire should be related to the level of

the rotational end restraints, which vary widely from PP to FF, and so the EC4 recommendations may not cover all cases. The ASCE Standard ASCE/SEI/SFPE 29-05 [47] considers the effects of different end conditions on the CFST columns exposed to fire using the effective length factors. However, as the design equation in ASCE/SEI/SFPE 29-05 originally came from the fire tests of CFST columns with the idealised PP and FF boundary conditions, no practical method exists in this standard for determining the high-temperature effective length factors of columns with various rotational restraints between PP and FF. A method for determining the buckling length of fire exposed TRC columns is proposed in this section, considering realistic rotational restraint levels.

For all the rotationally-restrained TRC columns investigated in Section 4.1, the high-temperature buckling length is defined as the distance between the bending moment zero points outputted in the FEA bending moment distributions. The buckling length ratios  $\mu_f$  of columns with various rotational restraint ratios  $\beta$  are shown in Fig. 19.  $\mu_f$  decreases from 1.0 to 0.5, as  $\beta$  increases from 0 to 5. The buckling length ratios for TRC columns with relatively large rotational end restraints (i.e.  $\beta > 5$  for the columns analysed in this study) are generally the same as those for the FF columns. The PF boundary option generates a buckling length ratio, which is approx. 0.7 at failure. The fire resistance of a column subject to lower load ratios is generally longer than that of the same column under higher load ratios, and so the buckling length of the former at failure is lower than that of the latter. This is because the buckling length of a heat-affected column generally decreases with the increase in the heating time, as presented in Fig. 16(i).

Another method to define the buckling lengths of rotationally-restrained columns is the equivalent length method. It is assumed that the buckling length of a restrained column is equal to the total length of an equivalent unrestrained column with the same fire resistance. However, this method is indirect and requires a lot of trial and error. The zero-moment method used in this study is compared with the equivalent length method in Fig. 20, for TRC columns of  $D = 600$  mm,  $\lambda = 30$  and  $50$ ,  $n = 0.5, 0.6$  and  $0.7$ . In general, these two methods result in almost identical buckling lengths, and so, the zero-moment method is recommended for determining the buckling length of TRC columns at failure.

The Chinese code JGJ 99-2015 [48] includes a method for determining the ambient-temperature buckling length of a steel column in a non-sway frame with different rotational restraint ratios. This method is further developed in this study for the determination of the high-temperature buckling length ratio  $\mu_f$  of square TRC columns at failure, as shown in Eq. (30). As mentioned in Section 2.1, only the square TRC columns with the same end rotational restraints are investigated in this study.

$$\mu_f = \frac{1 + 0.41\beta_t}{1 + 0.82\beta_t} \quad (30)$$

where  $\beta_t = (60a_{n,D}t + 1)\beta$ ;  $a_{n,D} = 0.094/D + n - 0.46$  and  $D$  is the cross-section size of the column in metres.

The buckling length ratios calculated using Eq. (30) are compared with the FEA results in Fig. 21(a). The average ratio between the calculated and FEA results is 1.01 with a standard deviation of 0.03, which verifies the suitability of Eq. (30).

After determining the buckling length  $L_{eff}$  of the TRC columns with different rotational restraints using Eq. (30), Eq. (8) proposed for the design of unrestrained columns in reference [12] can be extended for square TRC columns restrained rotationally. The buckling resistance values for the fire exposed rotationally restrained TRC columns calculated using Eq. (8) are compared in Fig. 21(b) with the applied axial loads in FEA. The buckling curve (c) of EC3 [45] is used for calculating the reduction coefficient of Eq. (21) for high temperatures. The good agreement between the calculated and FEA results, as shown in Fig. 21(b), confirms the suitability of the fire design method proposed as Eqs. (8) and (30) for square TRC columns with rotational restraints.

## 5. Effect of combined axial and rotational restraints

The fire behaviour of square TRC columns with combined axial and rotational restraints is studied in this section. The parameters considered are the cross-section size  $D$  (400 to 1500 mm), load ratio  $n$  (0.4 to 0.7), slenderness ratio  $\lambda$  (30 and 50), axial restraint ratio  $\alpha$  (0 to 0.1) and rotational restraint ratio  $\beta$  (0 to 0.5). The development of the axial deformation, lateral deformation, axial force ratio in the column, bending moment at column mid-height, column

top end rotation and bending moment in the end spring over time and the bending moment distribution along the column length at failure are based on the FEA. The results for an example column with  $D = 600$  mm,  $\lambda = 30$  and  $n = 0.6$  and with different end restraints are shown in Figs. 22 and 23.

Fig. 22 shows that, when the rotational restraint ( $\beta = 0.03$ ) is fixed and the axial restraint varies, the axial and lateral deformations, axial force, bending moment and column top end rotation decrease with an increase of the axial restraint ratio, which is observed also from the cases with axial restraints only ( $\beta = 0$ ). Fig. 22(g) shows that, for TRC columns with the same rotational restraint, the high-temperature buckling length at failure (i.e. distance between the bending moment zero points) decreases slightly when the axial restraint increases.

Fig. 23 shows the results when the axial restraint ( $\alpha = 0.03$ ) is fixed and the rotational restraint changes. As shown in Figs. 23(a) and 23(c), the variation of the rotational restraint has a negligible effect on the axial deformation and axial force, when the axial restraint remains unchanged. On the other hand, the lateral deformation, bending moment at column mid-height, column end rotation and buckling length at failure decrease significantly as the rotational restraint increases.

Fig. 24 presents the influence of axial and rotational restraint ratios on the fire resistance, axial force ratio and buckling length ratio at failure for the columns ( $D = 600$  mm,  $\lambda = 30$ ,  $n = 0.6$ ) with combined axial and rotational end restraints. These results are consistent with those discussed in Sections 3 and 4. In columns with identical rotational restraints, the fire resistance increases and both the axial force ratio and buckling length ratio at failure decrease, with the increase of the axial restraint ratio. In columns with identical axial restraints, the increase of the rotational restraint leads to an increase of the fire resistance and decreases of the axial force ratio and buckling length ratio at failure.

The applicability of the proposed design methods (Sections 3.3 and 4.3) to TRC columns with combined end restraints is assessed by including the effect of rotational restraint ratio  $\beta$  on the axial force ratio  $n_f$  at failure, and Eq. (7) is modified to Eq. (31). The axial force ratios at failure predicted by Eqs. (7) and (31) are verified against FEA results in Fig. 25(a). Eq. (31) provides a good match with the FEA results, whereas Eq. (7) overestimates  $n_f$ , especially

for columns with relatively high rotational restraints.

$$n_f = n - f(\beta) \cdot (3.6 - 0.047\lambda) \cdot \alpha \quad (31)$$

$$\text{where } f(\beta) = \begin{cases} 16\beta + 1 & \beta \leq 0.05 \\ 1.8 & \beta > 0.05 \end{cases} .$$

Since the enhancement of fire resistance due to the beneficial effect of axial restraint has already been considered in Eq. (30), this equation can be used directly for determining the buckling length ratio  $\mu_f$  at failure for columns with combined restraints. This has been verified against FEA, as shown in Fig. 25(b), indicating that a good agreement is reached.

It is expected that the buckling resistance determined using Eq. (8) and Eq. (30) and the axial force calculated using Eq. (31) are equal to each other at the failure time estimated by the FEA and this is verified in Fig. 25(c). The average of the ratios between the predicted buckling resistance and the calculated axial force at failure is 0.98 with a standard deviation of 0.10, confirming that the proposed design method is capable of determining the fire resistance of square TRC columns with combined end restraints. Fig. 26 presents the flow chart for the fire resistance design procedure of square TRC columns with axial and rotational end restraints.

## 6. Evaluation of temperature-dependent restraints

The axial and rotational restraints in the analysis conducted above are assumed to remain constant during heating. However, the surrounding structures adjacent to a heated TRC column may also be exposed to fire, causing the restraints at the column ends to vary with temperature. This section assesses the effects of temperature-dependent end restraints on the fire behaviour of square TRC columns.

### 6.1 Determination of temperature-dependent restraint stiffnesses

Yang et al. [12] have proposed a method for determining the equivalent flexural stiffness of a TRC section with obvious temperature gradients. Following the same approach, the high-temperature flexural stiffnesses of the connected RC beams can be determined as presented

next so as to determine the temperature-dependent restraining stiffnesses at the column ends. All the investigated rectangular RC beams are assumed to be exposed to ISO 834 standard fire [40] on three sides and have the same effective length to section depth ratio equal to 12. The width  $B_b$  of the beam cross-section varies from 200 mm to 600 mm and the depth-to-width ratio  $H_b/B_b$  changes from 2 to 3. The beams have rebars of 335 MPa yield strength and a nominal reinforcement ratio of 1.5%. The cylinder compressive strength of concrete is 40 MPa. The concrete cover of the reinforcing bars is 25 mm.

The flexural stiffness reduction  $k_{bFT}$  of the RC beams due to heating is obtained from the FEA and is shown in Fig. 27. As expected,  $k_{bFT}$  decreases as the temperature rises and  $k_{bFT}$  increases with the increasing beam width. Within the range analysed in this study, the influence of the depth-to-width ratio  $H_b/B_b$  on  $k_{bFT}$  is insignificant.

Eq. (32) is a regression formula for determining the evolution of  $k_{bFT}$  during heating. The reduction of the flexural stiffness over time according to Eq. (32) is compared with the FEA results in Fig. 27, indicating a good agreement.

$$k_{bFT} = 0.037t_B^4 - 0.289t_B^3 + 0.844t_B^2 - 1.206t_B + 1 \quad (32)$$

where  $t_B = t / (10B_b)^{0.5B_b+0.9}$ ;  $t$  is the duration of heating in hours and  $B_b$  is the beam width in metres.

## 6.2 Comparison with frame modelling

The modelling of the columns based on springs with temperature-dependent stiffness values is verified against a 2D frame model. The frame model is the same as that described in Section 2.3 except that the RC beams are heated at three sides. The temperature-dependent restraining stiffnesses of the end springs are determined using Eq. (32). To enable comparison, the beams of the frame model have linear elastic material properties, as considered in Eq. (32).

Fig. 28 shows the development of the axial deformation, lateral deformation and axial force over time and distributions of lateral deformations and bending moments along column length at failure for the TRC columns with temperature-dependent end springs, comparing well with those of the frame model. This figure indicates that the use of end springs with

temperature-dependent stiffnesses is effective in modelling the columns with heat-affected end restraints. Compared to the columns in Section 2.3 with constant end restraints, the fire resistance of a column with fixed bottom end decreases very slightly (by only 4.2%) when altering the spring stiffness from constant to temperature-dependent. For a column with pinned bottom end, the use of temperature-dependent spring stiffness results in a decrease in fire resistance by 7.0%, compared to the case with constant spring stiffness. The buckling length ratio at failure increases very slightly (1.6% for pinned bottom end, 2.8% for fixed bottom end), when altering the end restraint from constant to temperature-dependent.

### *6.3 Influence of temperature-dependent restraints*

The effects of temperature-dependent restraints on the fire behaviour of square TRC columns of 600 mm width are analysed in this section. The temperature-dependent restraint stiffnesses of the axial and rotational springs are restraint stiffnesses provided by the RC beams at ambient temperatures multiplied by  $k_{bFT}$  given in Eq. (32). Beams of different cross-section dimensions (200 × 500 mm, 300 × 700 mm and 400 × 1000 mm) are applied for achieving different restraint levels. Restraint B200×500-C is constant during heating, corresponding to a 200 × 500 mm beam, whereas B200×500-T is its temperature-dependent restraint counterpart.

#### *6.3.1 Effect of axial restraint*

The fire resistance  $t_{FR}$ , initial axial restraint ratio  $\alpha_i$ , axial restraint ratio  $\alpha_f$  at failure and axial force ratio  $n_f$  at failure for TRC columns with  $D = 600$  mm,  $n = 0.3, 0.5$  and  $0.7$  and  $\lambda = 30$  and  $50$  are summarised in Table 2 considering constant and temperature-dependent axial restraints.  $\alpha_i$  is the restraint ratio at ambient temperatures.  $\alpha_f$  is the ratio between the axial spring stiffness at failure and the column axial stiffness at ambient temperatures. Consistent with the observations in Section 3.2, the fire resistances of these columns increase approximately linearly with an increase in the initial axial restraint ratio. During heating, the restraint ratio decreases ( $\alpha_i$  is always larger than  $\alpha_f$ ). The effect of the temperature-dependant restraint is equivalent to that of a constant restraint which is in between  $\alpha_i$  and  $\alpha_f$ . Compared

to the cases with constant restraints, the effects of the temperature-dependent axial restraints on the fire resistance and axial force ratio at failure are generally insignificant, probably due to the small difference between  $\alpha_i$  and  $\alpha_f$  in these cases.

The development of the axial deformation, lateral deformation and axial force ratio over time for a few axially restrained TRC columns ( $D = 600$  mm,  $n = 0.5$  and  $\lambda = 30$  and  $50$ ) with constant and temperature-dependent axial end restraints is shown in Fig. 29. Compared to the cases with constant restraints, the temperature-dependent restraints result in small increases in the axial and lateral deformations, as well as slight decreases in the reduction of axial force during heating and in the fire resistance time.

### 6.3.2 Effect of rotational restraint

Table 3 summarizes the fire resistance  $t_{FR}$ , initial rotational restraint ratio  $\beta_i$ , rotational restraint ratio  $\beta_f$  at failure and buckling length ratio  $\mu_f$  at failure for TRC columns with  $D = 600$  mm,  $n = 0.5, 0.6$  and  $0.7$  and  $\lambda = 30$  and  $50$ , assuming constant and temperature-dependent rotational restraints.

The initial and failure rotational restraint ratios  $\beta_i$  and  $\beta_f$  are defined similarly as for  $\alpha_i$  and  $\alpha_f$ , described in Section 6.3.1. The rotational restraint ratio decreases with the increasing temperature, hence  $\beta_i$  is always larger than  $\beta_f$ . As previously discussed in Section 4.2 (Fig. 18), the beneficial effect of the constant rotational restraint in enhancing the fire resistance of the column is particularly significant when  $\beta$  is between 0 and 0.5 and the fire resistance values for the columns with  $\beta \geq 0.5$  are almost identical. The difference in fire resistance values between the cases of constant and temperature-dependent rotational restraints is insignificant, when  $\beta_i$  and  $\beta_f$  are both greater than 0.5. However, when both of them are in the range of 0 to 0.5, the difference in the fire resistance values between the cases with constant and temperature-dependent rotational restraints is generally considerable. An example of the columns in Table 3 shows that for the ones with  $\lambda = 50$  and  $n = 0.6$  and with restraints B200×500-C and B200×500-T, the fire resistance decreases from 233.4 minutes to 172 minutes (-26%) and the buckling length ratio at failure increases from 0.529 to 0.615 as the type of the rotational restraint changes from constant to temperature-dependent.

Fig. 30 presents the development of the axial and lateral deformations over time, and the distributions of lateral deformations and bending moments along the column length at failure for 12 TRC columns ( $D = 600$  mm,  $n = 0.6$  and  $\lambda = 30$  &  $50$ ) with constant and temperature-dependent rotational end restraints. Figs. 30(a) and 30(b) show that the lateral deformations are more affected by the reduction of the rotational stiffness during heating than the axial deformations. Figs. 30(c) and 30(d) indicate that the bending moments and lateral deformations, both at column mid height and at failure time, of the cases with temperature-dependent rotational restraints are larger than those of the cases with constant restraints. The differences in deformations and bending moments between the cases with constant and temperature-dependent rotational restraints are insignificant for most of the investigated columns, except for those with the initial rotational restraint ratios  $< 0.5$ .

## 7. Conclusions

The fire behaviour of square TRC columns in non-sway frames has been investigated with the aid of FEA modelling, where the end restraints of the column are modelled using the axial and rotational springs in ABAQUS. To study the influences of the cross-section size, slenderness ratio, load ratio, axial and rotational restraint ratios on the fire resistance of the columns, parametric analyses have been carried out. Based on the FEA results, the following conclusions can be drawn:

- (1) The FEA model developed in this study yields good predictions compared with the fire test results for the restrained CFST columns. The restraints provided by the adjacent structures to a heated column could be modelled effectively using rotational and axial springs with either constant or temperature-dependent stiffnesses;
- (2) Axial end restraint may lead to a decrease in the axial force and an increase in the fire resistance of TRC columns. The fire resistance of axially-restrained square TRC columns increases almost linearly with the increase of the axial restraint ratio. The average enhancement of fire resistance ranges from 11.2% to 61.8% with axial restraint ratios in the range of 0.01 to 0.05;
- (3) Rotational restraint may decrease the mid-height bending moment and buckling length

- and increase the fire resistance time of the column. The increase in fire resistance caused by a stepwise increase of the rotational restraint is the largest when the restraint ratio is relatively low (0 to 0.5). The fire resistance of a column with a rotational restraint ratio higher than 5 is nearly the same as that of a column with fixed-fixed boundary conditions;
- (4) A design method for the fire design of end-restrained square TRC columns has been developed;
- (5) The use of temperature-dependent end restraints (either axial or rotational), instead of constant ones, leads to a decrease in the fire resistance of the column. The magnitude of this decrease depends mainly on the variability of the restraint during heating and is generally less than 10%.

## Acknowledgements

The research work in this paper is financially supported by the National Natural Science Foundation of China (51878220), to which the authors are grateful.

## References

- [1] Zhou XH, Liu JP. Performance and design of steel tube confined concrete members. Beijing China: Science Press Ltd.; 2010 [in Chinese].
- [2] M. Tomii, K. Sakino, K. Watanabe, Y. Xiao, Lateral load capacity of reinforced concrete short columns confined by steel tube, Proceedings of the International Speciality Conference on Concrete Filled Steel Tubular Structures, Harbin, China (1985), 19-26
- [3] R.S. Aboutaha, R.I. Machado, Seismic resistance of steel-tubed high-strength reinforced-concrete columns, *J. Struct. Eng.* 125 (5) (1999) 485-494.
- [4] K. Lahlou, M. Lachemi, P.C. Aïtcin, Confined high-strength concrete under dynamic compressive loading, *J. Struct. Eng.* 125(10) (1999) 1100-1108.
- [5] Y.P. Sun, K. Sakino, Earthquake-resisting performance of RC columns confined by square steel tube, Part 3: effects of shear span ratio of column, *J. Struct. Constr. Eng. AIJ.* 547 (2001) 129-136.

- [6] L.H. Han, G.H. Yao, Z.B. Chen, Q. Yu, Experimental behaviours of steel tube confined concrete (STCC) columns, *Steel Compos. Struct.* 5 (6) (2005) 459-484.
- [7] S.M. Zhang, J.P. Liu, Seismic behavior and strength of square tube confined reinforced-concrete (STRC) columns, *J. Constr. Steel Res.* 63 (9) (2007) 1194-1207.
- [8] X.D. Wang, J.P. Liu, S.M. Zhang, Behavior of short circular tubed-reinforced-concrete columns subjected to eccentric compression, *Eng. Struct.* 105 (2015) 77-86.
- [9] JGJ/T471, Technical Standard for Steel Tube Confined Concrete Structures, MOHURD (Ministry of Housing and Urban-Rural Development of the People's Republic of China), Beijing, China, 2020 [In Chinese]
- [10] F.Q. Liu, Y.Y. Wang, L. Gardner, A.H. Varma, Experimental and numerical studies of reinforced concrete columns confined by circular steel tubes exposed to fire, *J. Struct. Eng.* 145 (11) (2019) 04019130.
- [11] D.D. Yang, F.Q. Liu, S. Huang, H. Yang, ISO 834 standard fire test and mechanism analysis of square tubed-reinforced-concrete columns, *J. Constr. Steel Res.* 175 (2020) 106316.
- [12] D.D. Yang, F.Q. Liu, S. Huang, H. Yang, Structural fire safety design of square and rectangular tubed-reinforced-concrete columns, *Structures.* 29 (2021) 1286-1321.
- [13] J. Janss, R. Minne, Buckling of steel columns in fire conditions, *Fire Safety J.* 4 (4) (1981) 227-235.
- [14] Y.C. Wang, T. Lennon, D.B. Moore, The behavior of steel frames subject to fire, *J. Constr. Steel Res.* 35 (1995) 291–322.
- [15] Y.C. Wang, Effects of structural continuity on the fire resistance design of steel columns in non-sway multi-storey frames, *Fire Safety J.* 28 (1997) 101–116.
- [16] J.C. Valente, I.C. Neves, Fire resistance of steel columns with elastically restrained axial elongation and bending, *J. Constr. Steel Res.* 52 (3) (1999) 319-331.
- [17] Shepherd P. The performance in fire of restrained columns in steel-framed construction. Doctoral dissertation, Sheffield, University of Sheffield, 1999.
- [18] F. Ali, D. O'Connor, Structural performance of rotationally restrained steel columns in fire, *Fire Safety J.* 36(7) (2001) 679-691.

- [19] F.A. Ali, P. Shepherd, M. Randall, I.W. Simms, D.J. O'Connor, I. Burgess, The effect of axial restraint on the fire resistance of steel columns, *J. Constr. Steel Res.* 46(1–3) (1998) [paper no.177]
- [20] F.C.T. Gomes, P.M.P.E. Costa, J.P.C. Rodrigues, I.C. Neves, Buckling length of a steel column for fire design, *Eng. Struct.* 29 (2007) 2497–2502.
- [21] T. Hozjan, I. Planinc, M. Saje, S. Srpacic, Buckling of restrained steel columns due to fire conditions, *Steel Compos. Struct.* 8(2) (2008) 159-178.
- [22] P.G. Shepherd, I.W. Burgess, On the buckling of axially restrained steel columns in fire, *Eng. Struct.* 33 (2011) 2832–2838.
- [23] A.M. Correia, J.P. Rodrigues, Fire resistance of steel columns with restrained thermal elongation, *Fire Safety J.* 50 (2012) 1–11.
- [24] C. Couto, P. Vila Real, N. Lopes, J.P. Rodrigues, Buckling analysis of braced and unbraced steel frames exposed to fire, *Eng. Struct.* 49 (2013) 541–559.
- [25] Y.C. Wang, The effects of structural continuity on the fire resistance of concrete filled columns in non-sway frames, *J. Constr. Steel Res.* 50 (1999) 177–197.
- [26] C. Bailey, Effective lengths of concrete-filled steel square hollow sections in fire, *Struct. Build.* 140 (2) (2000) 169–178.
- [27] A.J.P.M. Correia, J.P.C. Rodrigues, Fire resistance of partially encased steel columns with restrained thermal elongation, *J. Constr. Steel Res.* 67(4) (2011) 593-601.
- [28] T.A.C. Pires, J.P.C. Rodrigues, J.J.P. Silva, Fire resistance of concrete filled circular hollow columns with restrained thermal elongation, *J. Constr. Steel Res.* 77 (2012) 82-94.
- [29] J.P.C. Rodrigues, L. Laim, Fire resistance of restrained composite columns made of concrete filled hollow sections, *J. Constr. Steel Res.* 133 (2017) 65-76.
- [30] J.P.C. Rodrigues, L. Laim, Fire response of restrained composite columns made with concrete filled hollow sections under different end-support conditions, *Eng. Struct.* 141 (2017) 83-96.
- [31] C. Ibañez, M.L. Romero, A. Hospitaler, Effects of axial and rotational restraints on concrete-filled tubular columns under fire, *J. Constr. Steel Res.* 125 (2016) 114-127.

- [32] B. Young, E. Ellobody, Performance of axially restrained concrete encased steel composite columns at elevated temperatures, *Eng. Struct.* 33(1) (2011) 245-254.
- [33] F.Q Liu, Y.C Pan, H. Yang, FEA on mechanical behaviour of axially restrained concrete-filled steel tubular columns subjected to fire, *J. Build. Struct.* 36(S1) (2015) 310-317. [In Chinese]
- [34] G.Y Wang, C.H Qiu, L. Wang, Fire performance of end-restrained concrete filled steel tubular columns, *Build. Struct.* 48(4) (2018) 50-55. [In Chinese]
- [35] T.T. Lie, Fire resistance of circular steel columns filled with bar-reinforced concrete, *J. Struct. Eng.* 120 (1994) 1489-1509.
- [36] ASCE, Structural fire protection. Manual of Practice No. 78, ASCE, Reston, VA, 1992.
- [37] S. Hong, A.H. Varma, Analytical modeling of the standard fire behavior of loaded CFT columns, *J. Constr. Steel Res.* 65 (2009) 54-69.
- [38] EN 1992-1-2, Eurocode 2 - Design of Concrete Structures - Part 1-2: General Rules - Structural Fire Design, CEN, Brussels, 2004.
- [39] EN 1993-1-2, Eurocode 3 - Design of Steel Structures - Part 1-2: General Rules - Structural Fire Design, CEN, Brussels, 2005.
- [40] ISO 834-1, Fire Resistance Test - Elements of Building Construction, Part 1: General Requirements, International Organization for Standardization ISO 834, Geneva, Switzerland, 1999.
- [41] B. Wu, C.J Qiao, Axial force in restrained RC columns during heating and cooling phase, *J. Civ. Arc. & Env. Eng.* 32(2) (2010) 53-59. [In Chinese]
- [42] JGJ 3, Technical Specification for Concrete Structures of Tall Building, MOHURD (Ministry of Housing and Urban-Rural Development of the People's Republic of China), Beijing, China, 2011 [In Chinese]
- [43] GB 50010, Codes for Design of Concrete Structures, MOHURD (Ministry of Housing and Urban-Rural Development of the People's Republic of China), Beijing, China, 2015 [In Chinese]
- [44] EN 1994-1-2, Eurocode 4 - Design of Composite Steel and Concrete Structures - Part 1-2: General Rules - Structural Fire Design, CEN, Brussels, 2008.

- [45] EN 1993-1-1, Eurocode 3 - Design of Steel Structures - Part 1-1: General Rules and Rules for Buildings, CEN, Brussels, 2005.
- [46] GB 50936, Technical Code for Concrete Filled Steel Tubular Structures, MOHURD (Ministry of Housing and Urban-Rural Development of the People's Republic of China), Beijing, China, 2014 [In Chinese]
- [47] ASCE/SEI/SFPE 29-05, Standard calculation methods for structural fire protection. ASCE, Reston, VA, 2007.
- [48] JGJ 99-2015, Technical Specification for Steel Structure of Tall Building, MOHURD (Ministry of Housing and Urban-Rural Development of the People's Republic of China), Beijing, China, 2016 [In Chinese]

## Figures

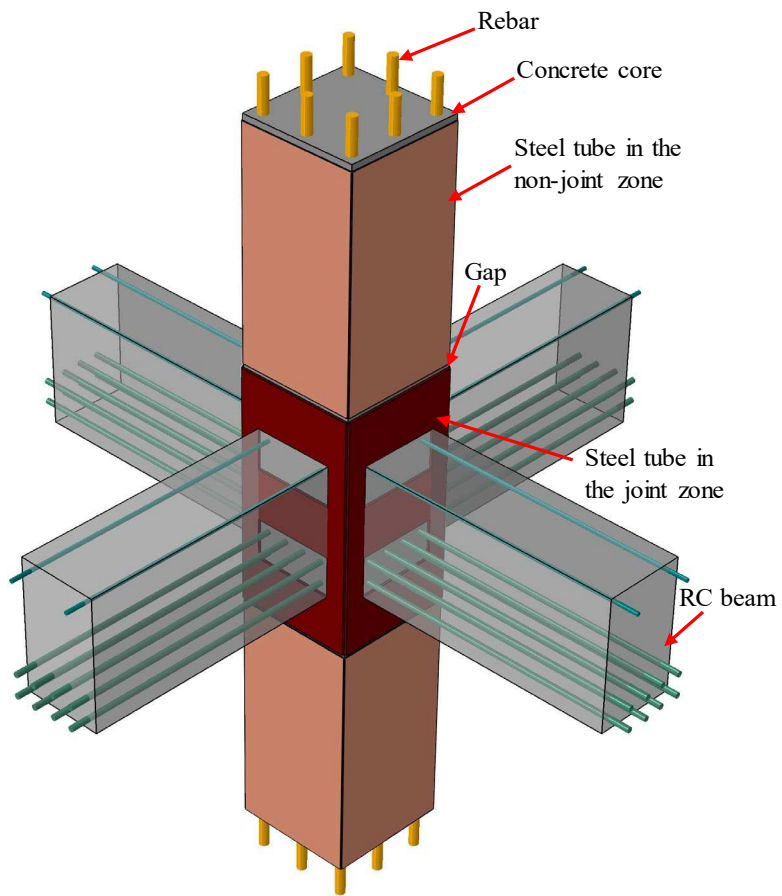


Fig. 1. Schematic view of the square TRC columns

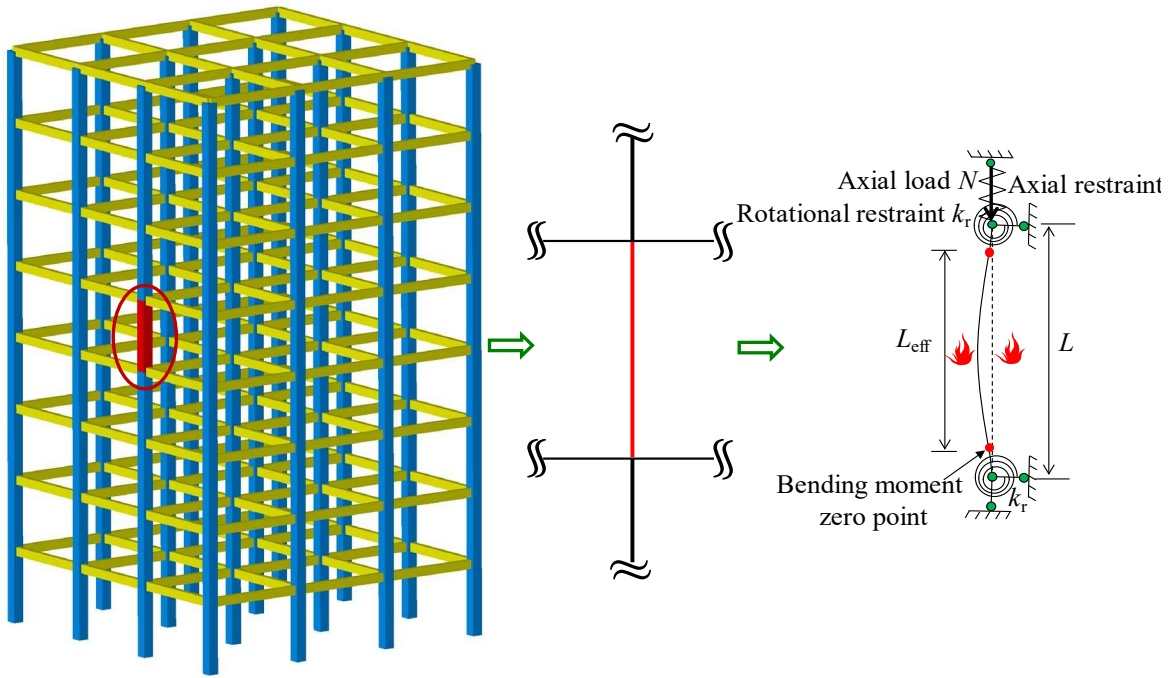


Fig. 2. Simplification of column end restraints in the frame

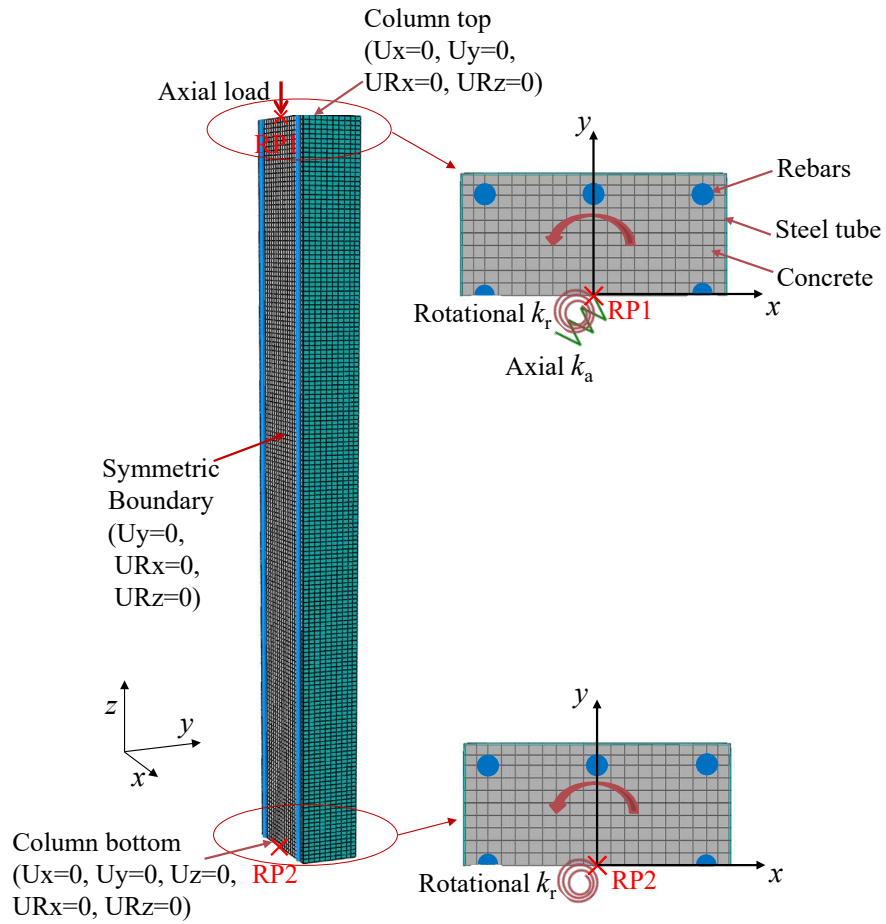
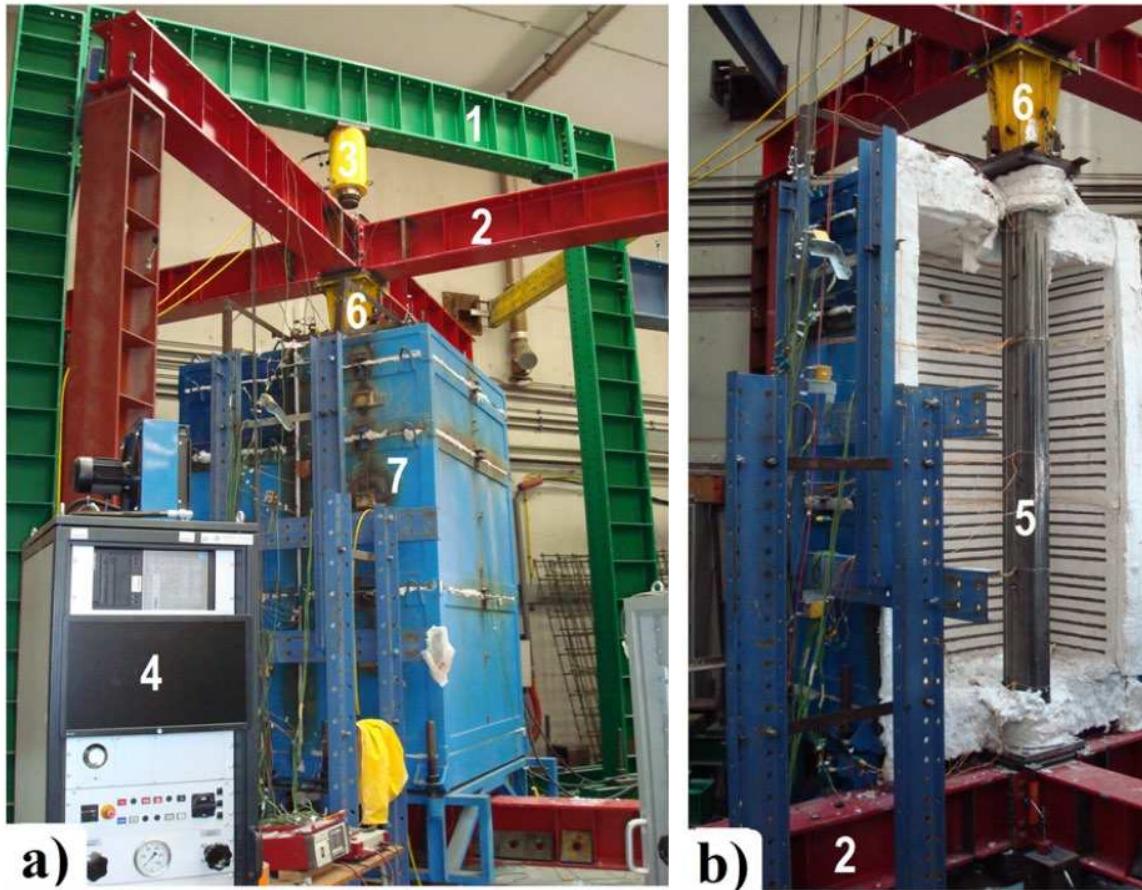


Fig. 3. Modelling of the column end restraints in FEA using axial and rotational springs



(a) General view [29]

(b) Detailed view [29]

Fig. 4. General and detailed views of the setup for the tests of CFST columns conducted in reference [29]: 1 - reaction frame; 2 - restraining frame; 3 - hydraulic jack; 4 - servo hydraulic central unit; 5 - specimen; 6 - restraining forces measuring device; 7 - electric furnace

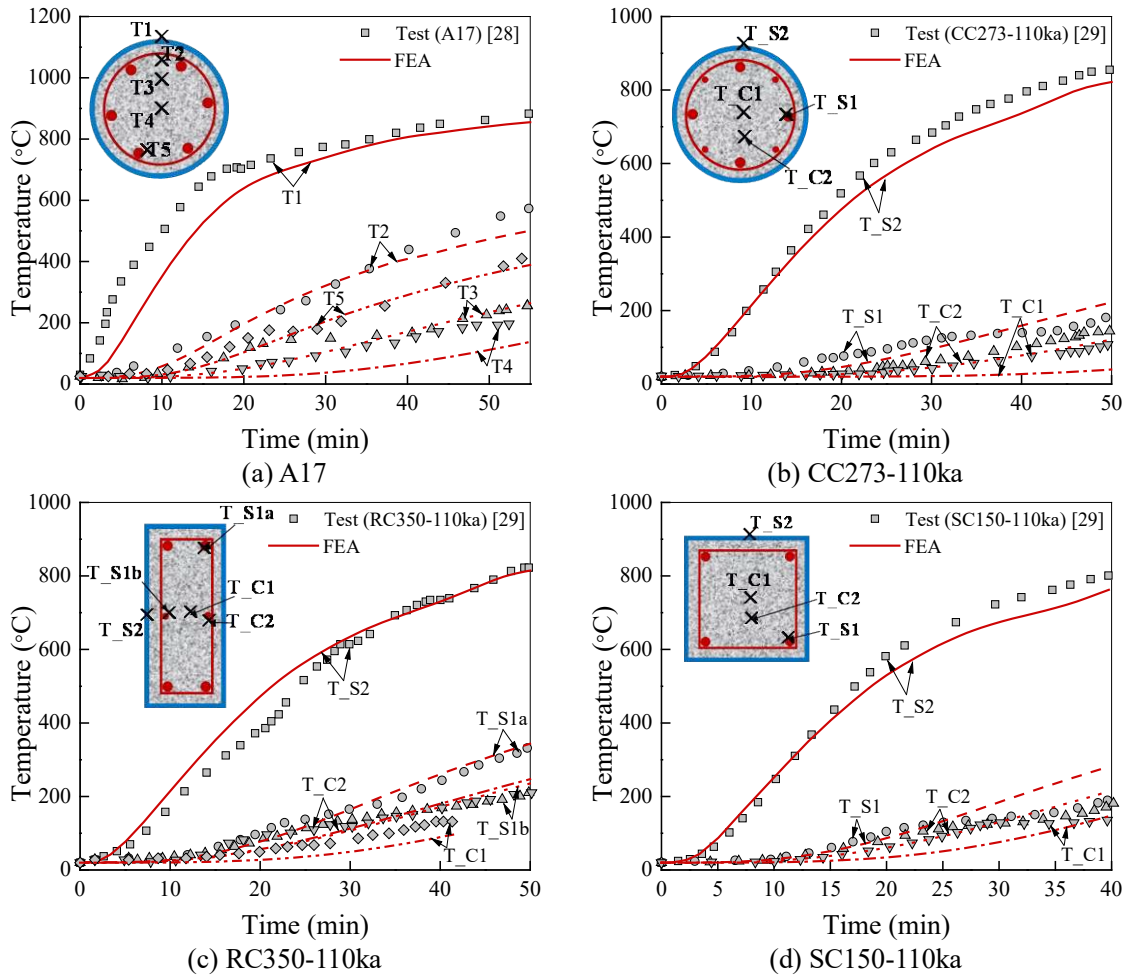
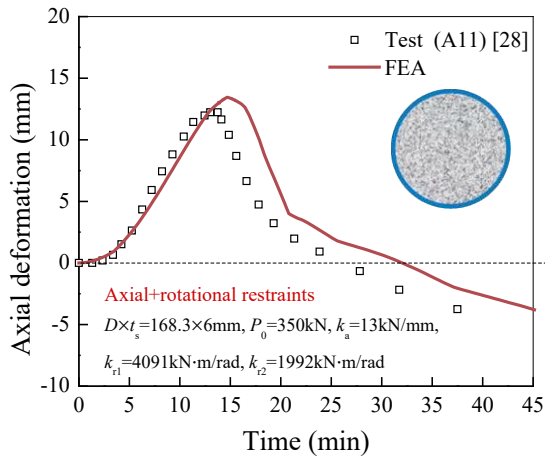
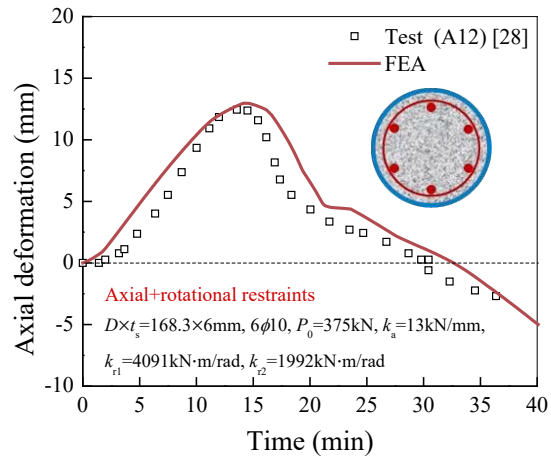


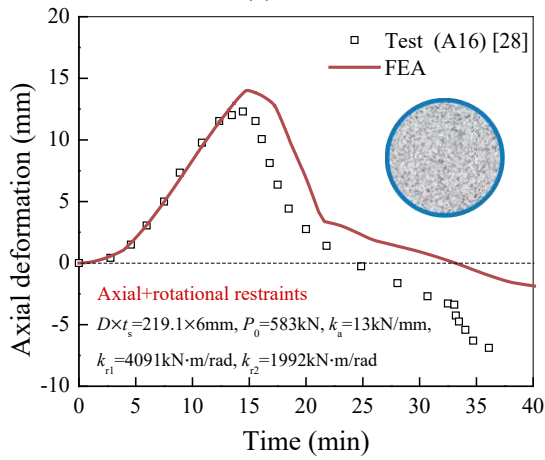
Fig. 5. The development of temperature over time in restrained CFST columns – FEA vs fire tests



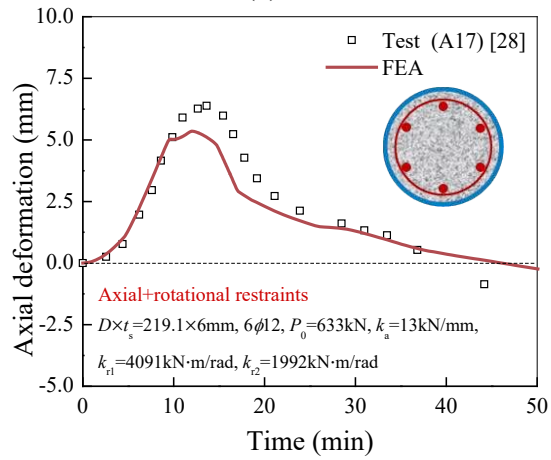
(a) A11



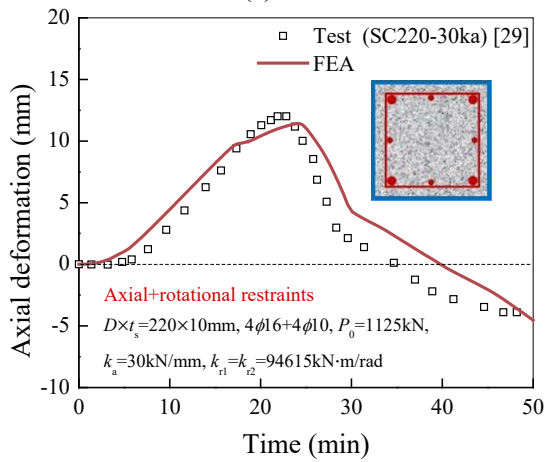
(b) A12



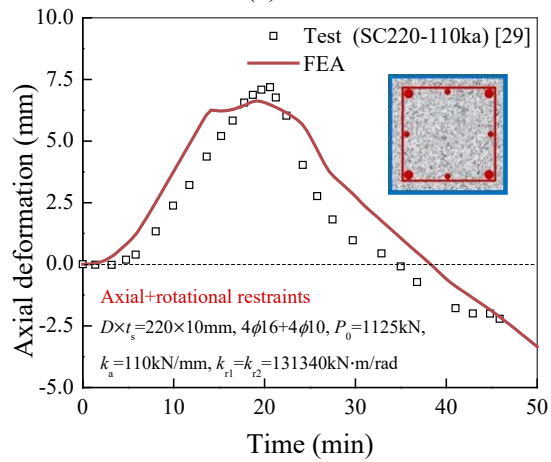
(c) A16



(d) A17

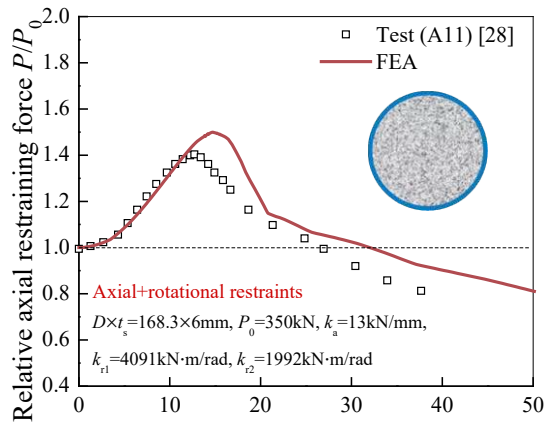


(e) SC220-30ka

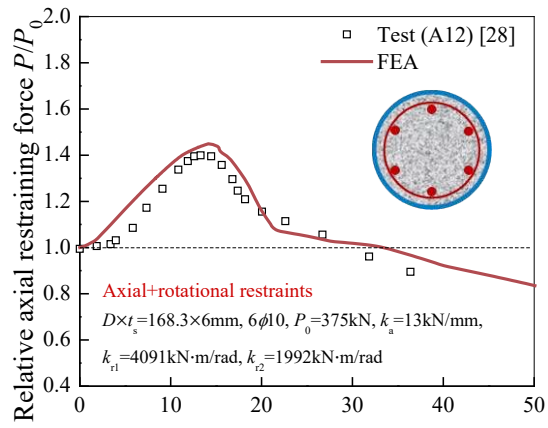


(f) SC220-110ka

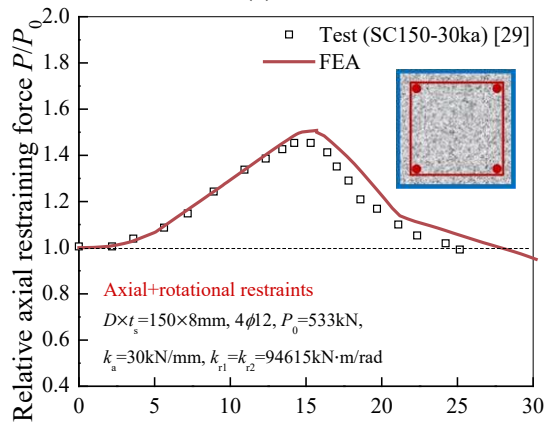
Fig. 6. The development of axial deformation over time in restrained CFST columns – FEA vs fire tests



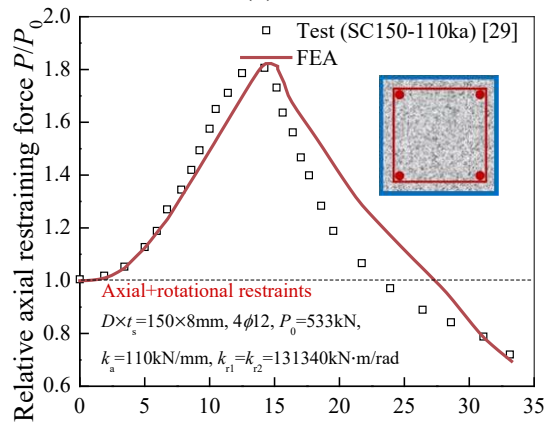
(a) A11



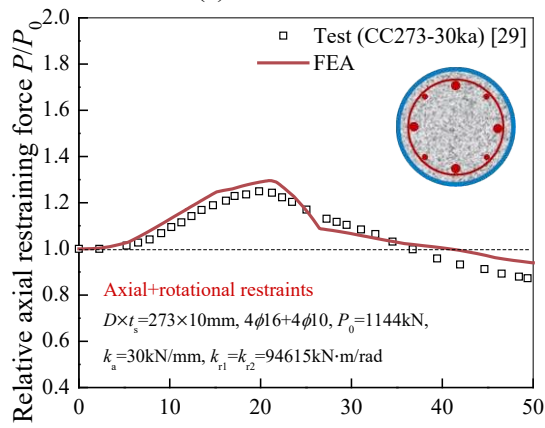
(b) A12



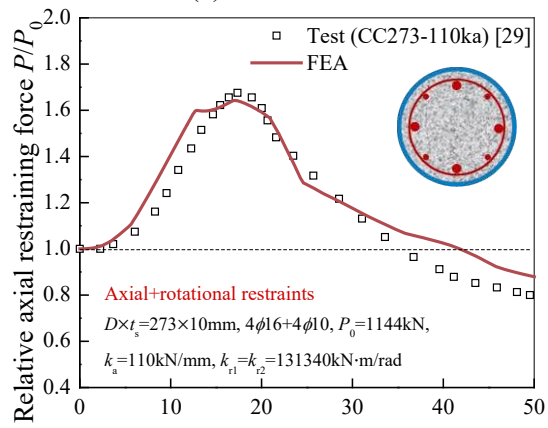
(c) SC150-30ka



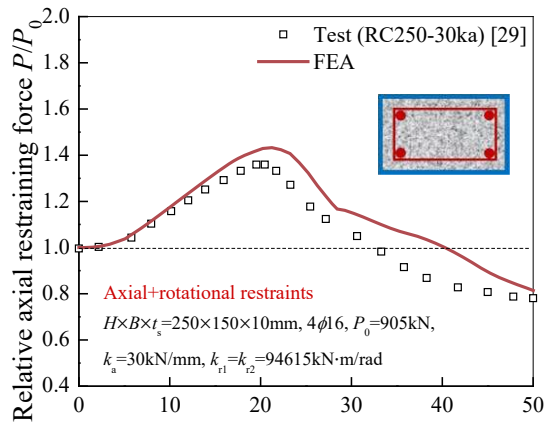
(d) SC150-110ka



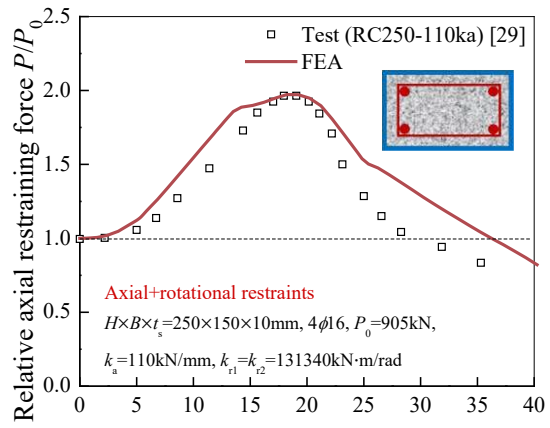
(e) CC273-30ka



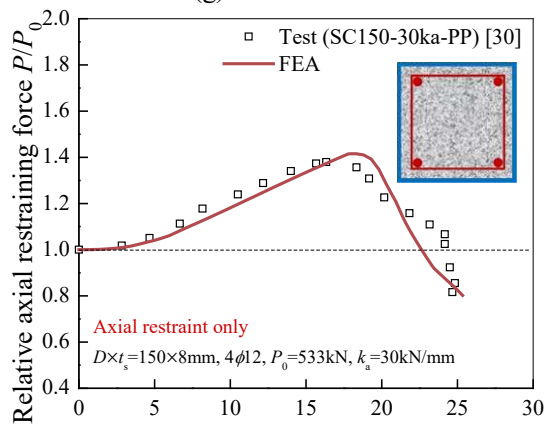
(f) CC273-110ka



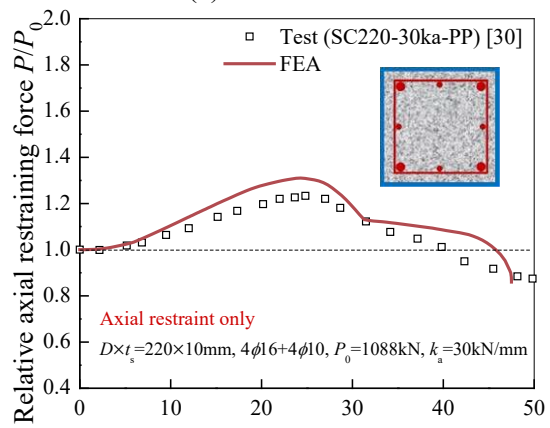
(g) RC250-30ka



(h) RC250-110ka



(i) SC150-30ka-PP



(j) SC220-30ka-PP

Fig. 7. The development of relative axial restraining force over time in restrained CFST columns – FEA vs fire tests

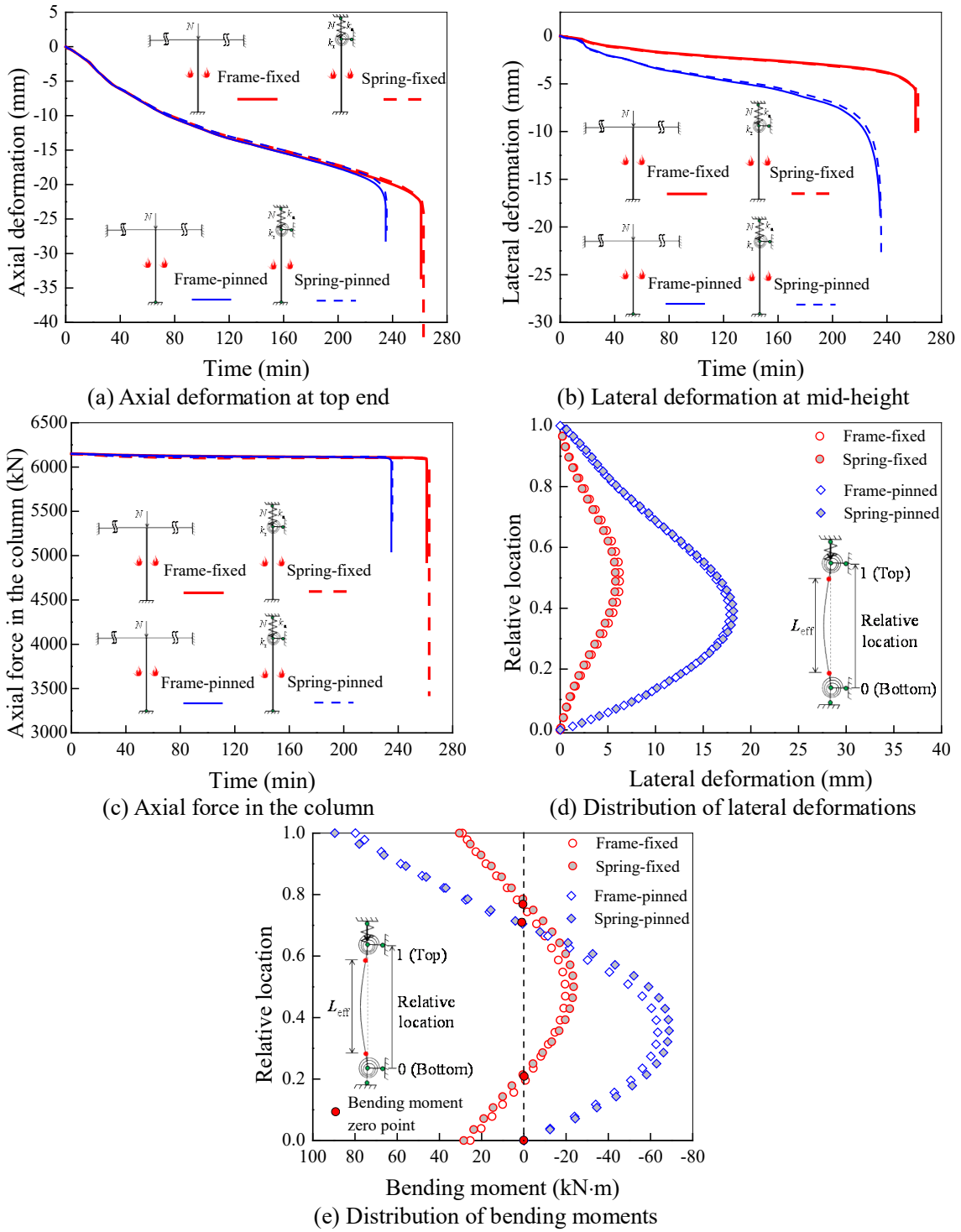
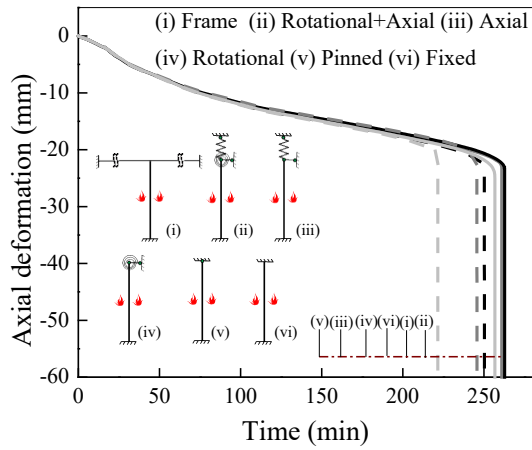
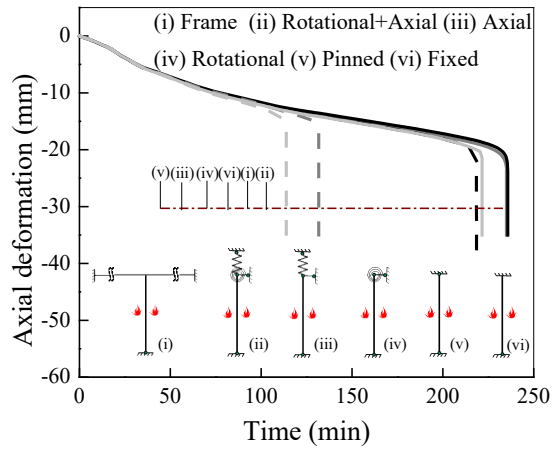


Fig. 8. Validation of the spring model against the frame modelling with unheated beams



(a) Bottom of the column fixed



(b) Bottom of the column pinned

Fig. 9. Influence of boundary conditions and end restraints on axial deformations

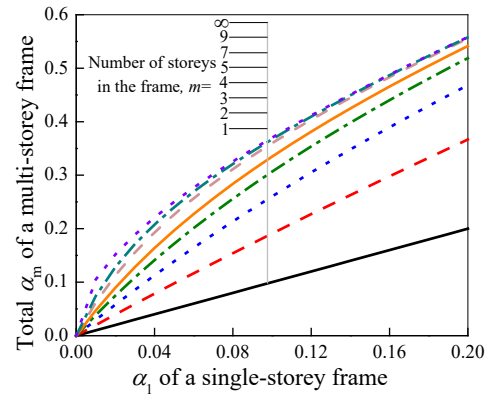


Fig. 10. Axial restraint ratio of a column in a multi-storey frame

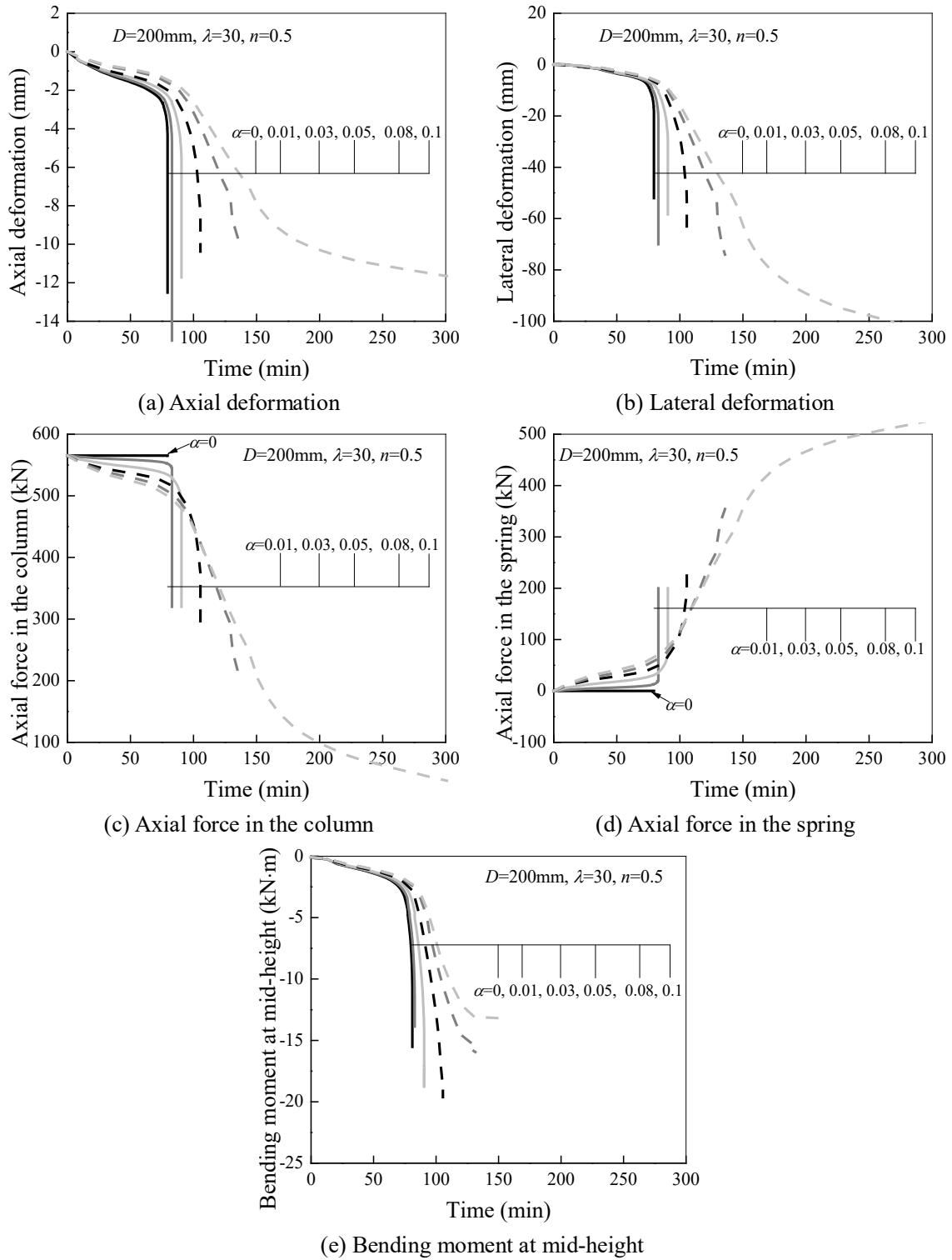


Fig. 11. Overall deformations, axial forces and bending moments in axially restrained TRC columns ( $D = 200 \text{ mm}$ ,  $\lambda = 30$ ,  $n = 0.5$ )

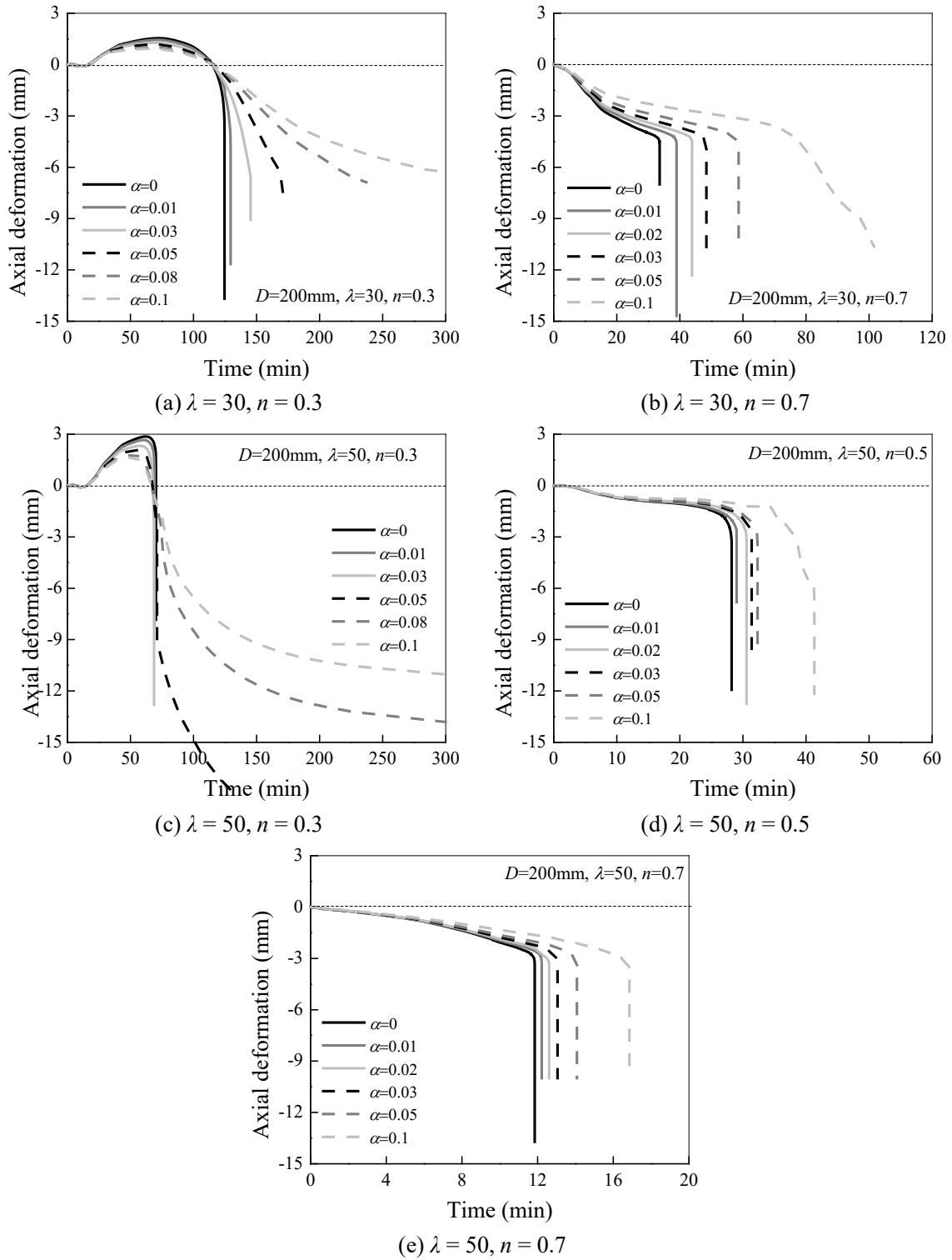


Fig. 12. Axial deformation vs. time relationships for axially-restrained TRC columns ( $D = 200$  mm)

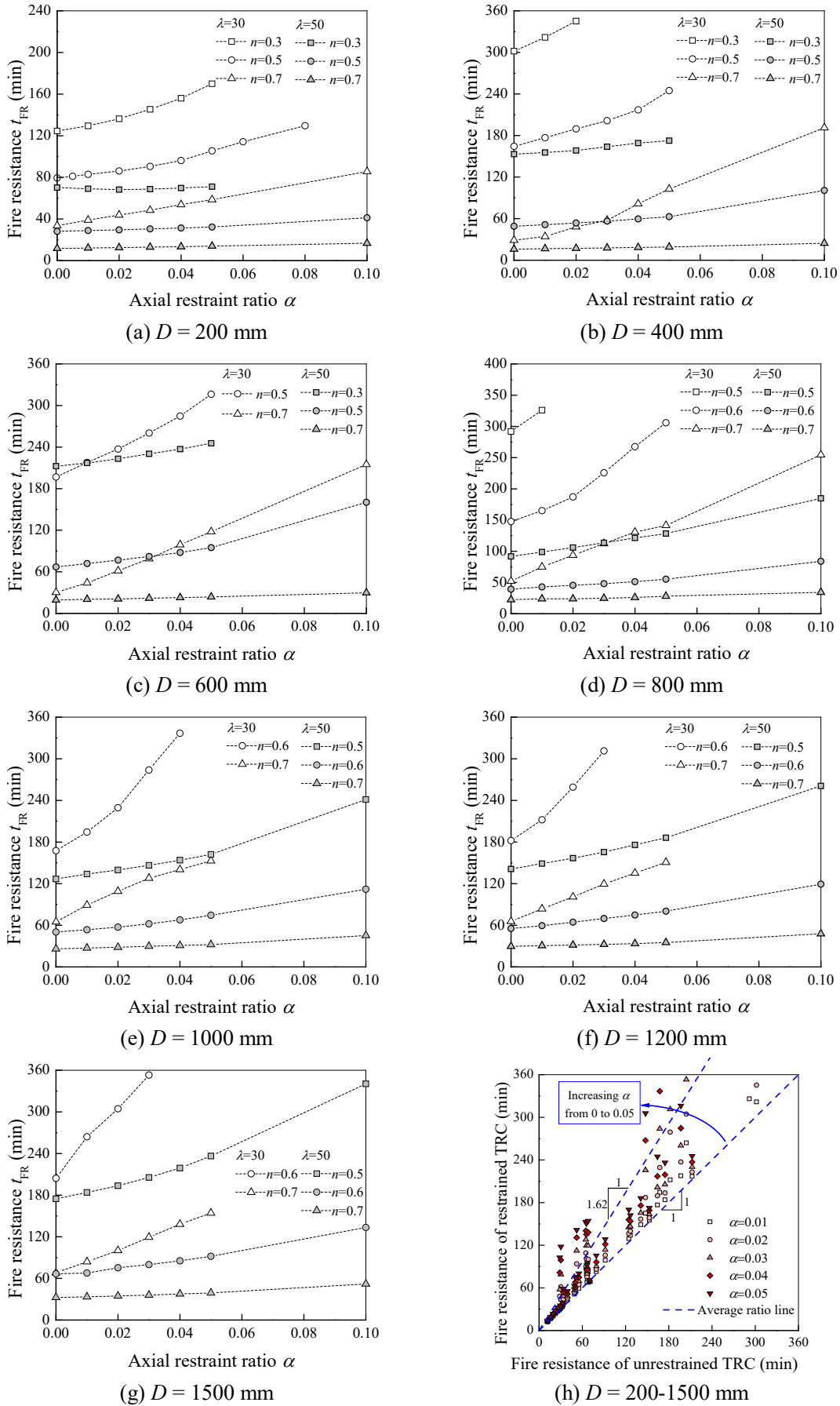


Fig. 13. Influence of axial restraint ratio on the fire resistance of axially-restrained TRC columns

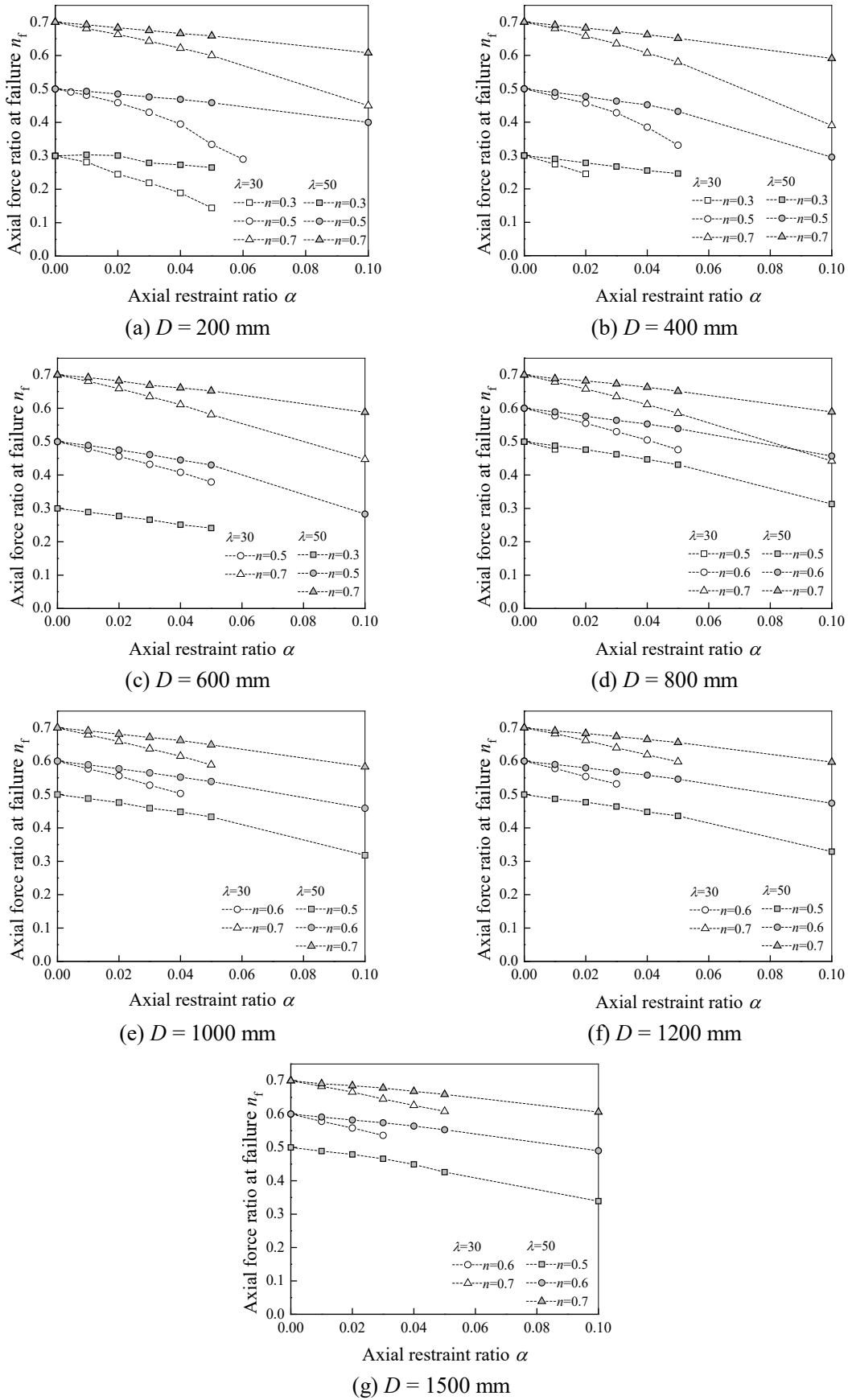
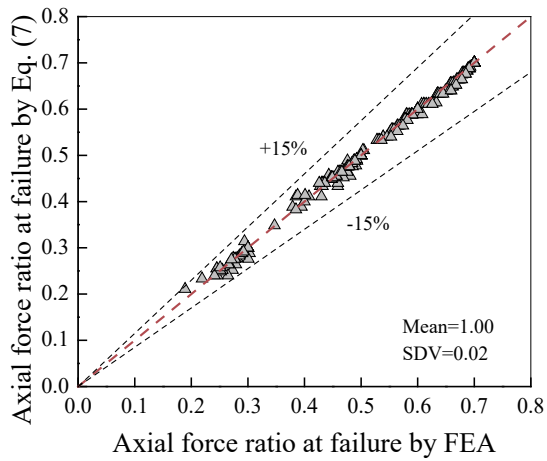
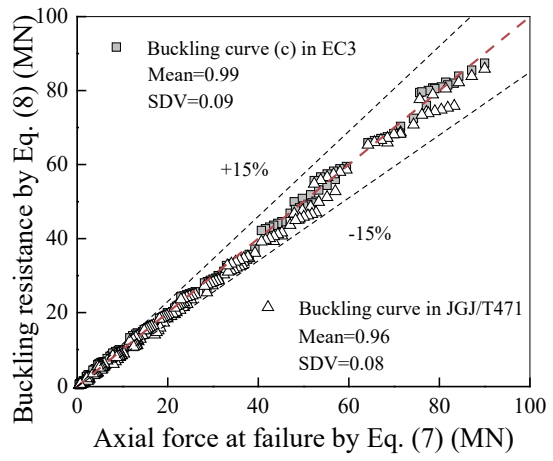


Fig. 14. Influence of axial restraint ratio on the axial force ratio at failure for axially restrained columns

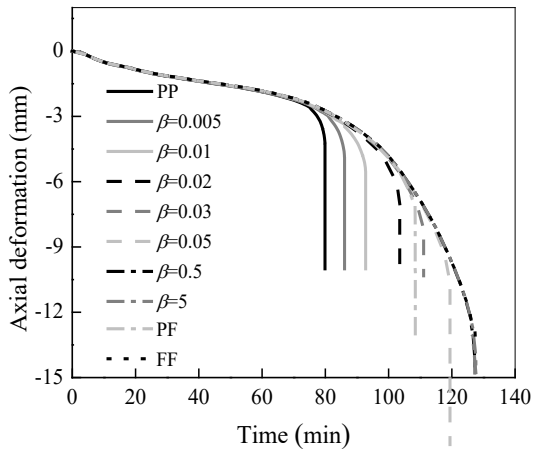


(a) Axial force ratio at failure

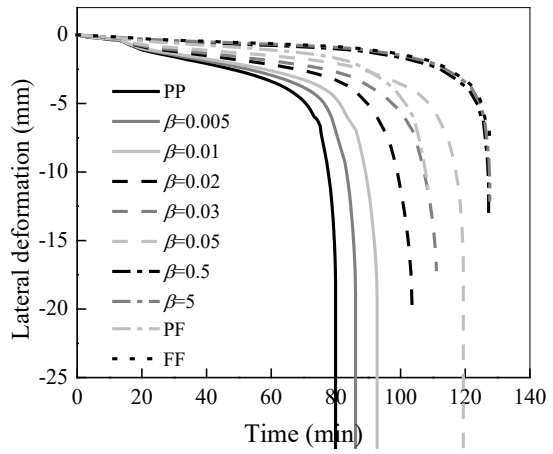


(b) Buckling resistance

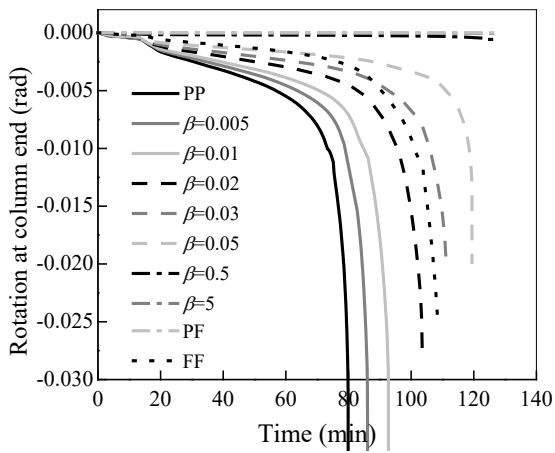
Fig. 15. Predicted axial force ratio at failure and buckling resistance using the proposed design method



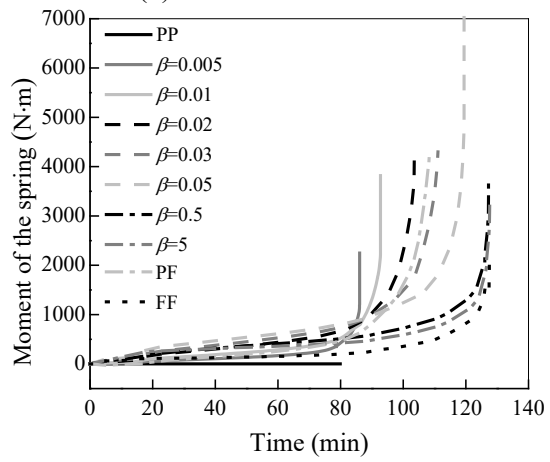
(a) Axial deformation



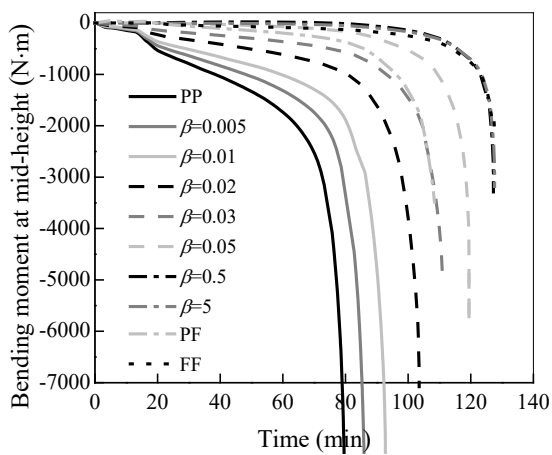
(b) Lateral deformation



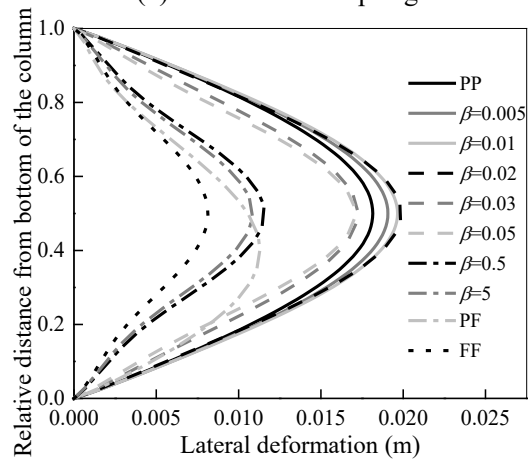
(c) Rotation at column end



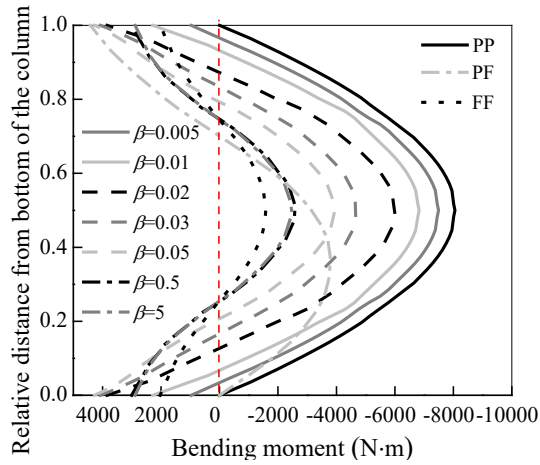
(d) Moment in the spring



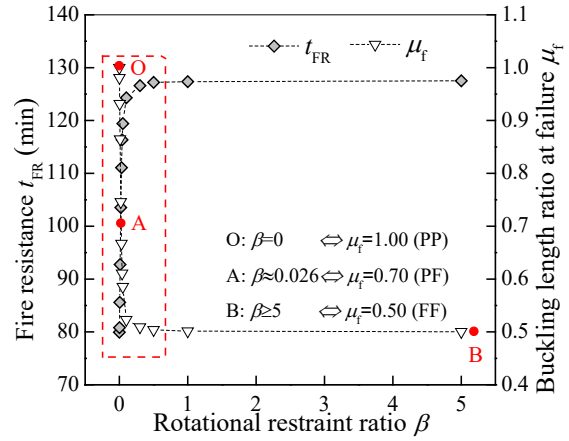
(e) Bending moment at mid-height



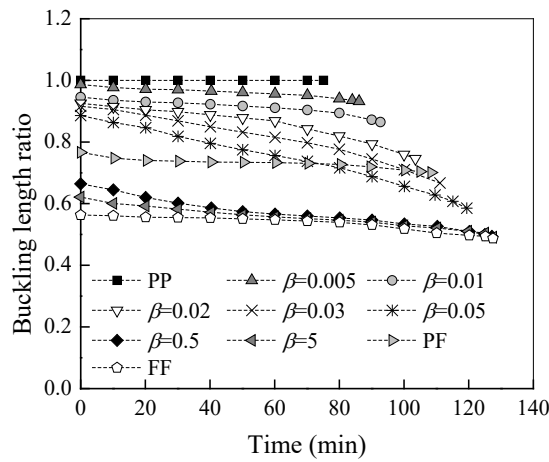
(f) Distribution of lateral deformations



(g) Distribution of bending moments



(h) Fire resistance & Buckling length ratio at failure



(i) Buckling length ratio vs time

Fig. 16. Influence of rotational restraint ratio on the fire performance of rotationally-restrained columns ( $D = 200 \text{ mm}$ ,  $\lambda = 30$ ,  $n = 0.5$ )

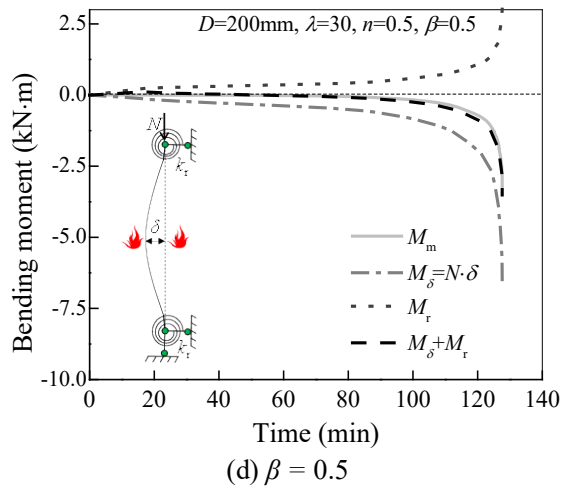
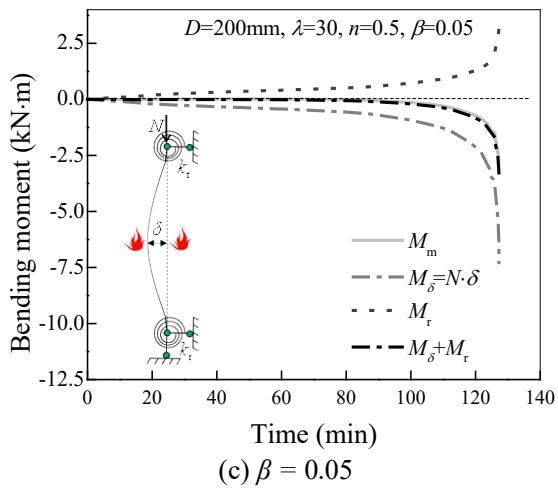
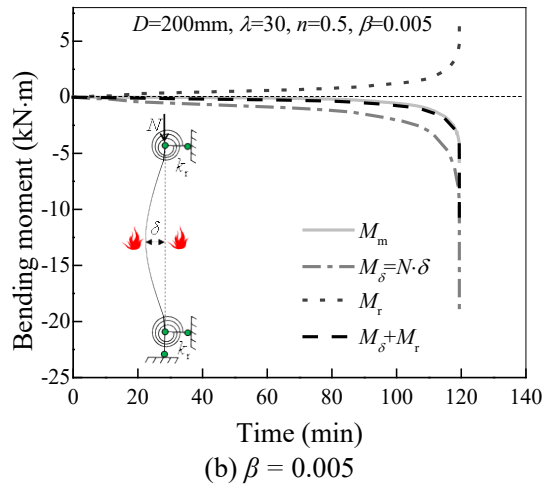
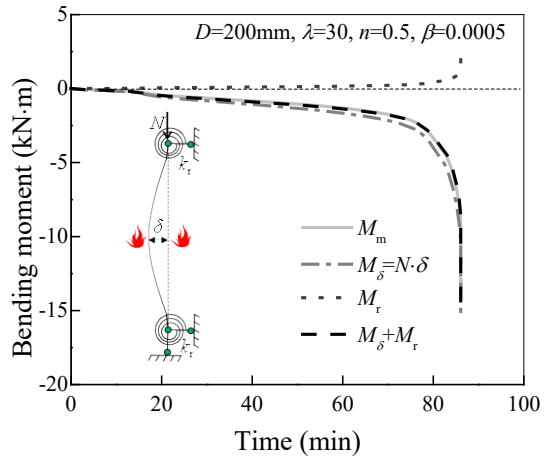
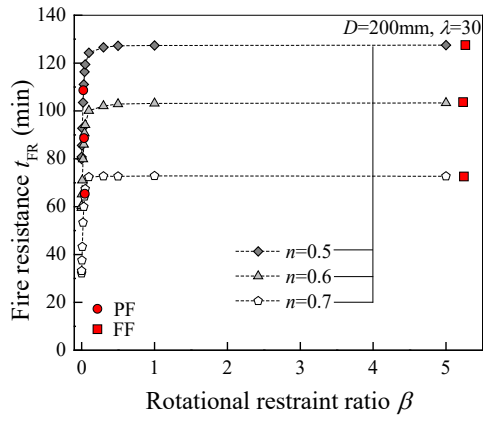
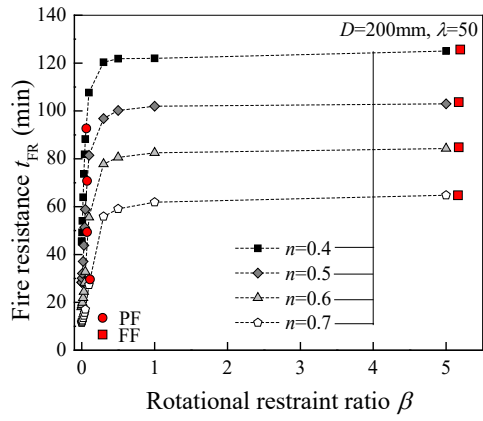


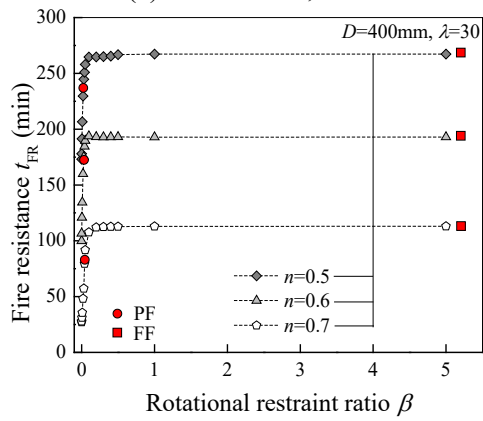
Fig. 17. Effect of rotational restraint on the bending moment at mid-height of the column ( $D = 200 \text{ mm}, \lambda = 30, n = 0.5$ )



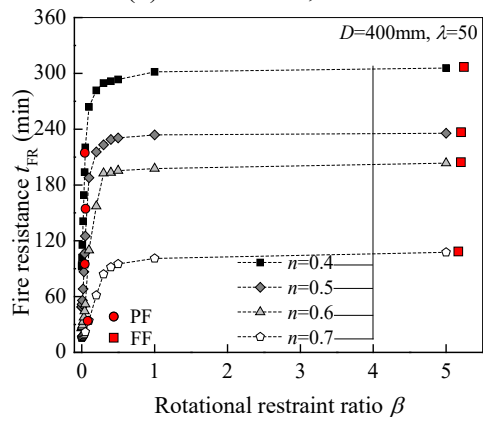
(a)  $D = 200 \text{ mm}, \lambda = 30$



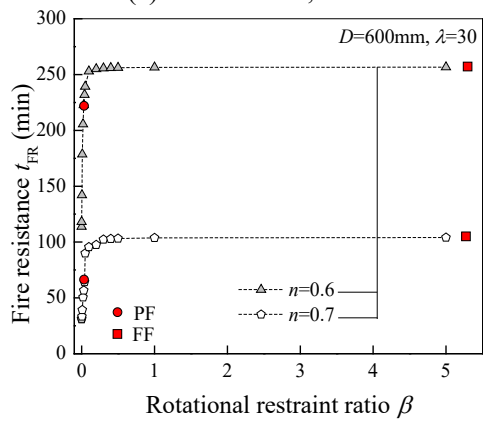
(b)  $D = 200 \text{ mm}, \lambda = 50$



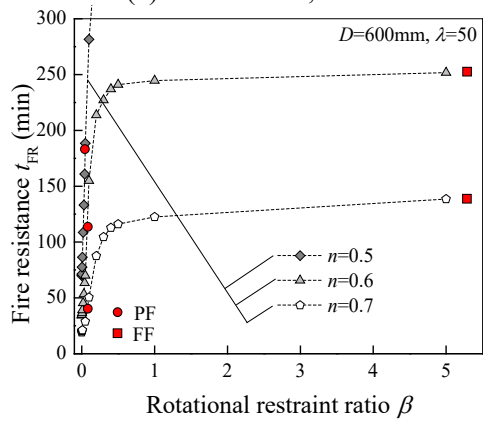
(c)  $D = 400 \text{ mm}, \lambda = 30$



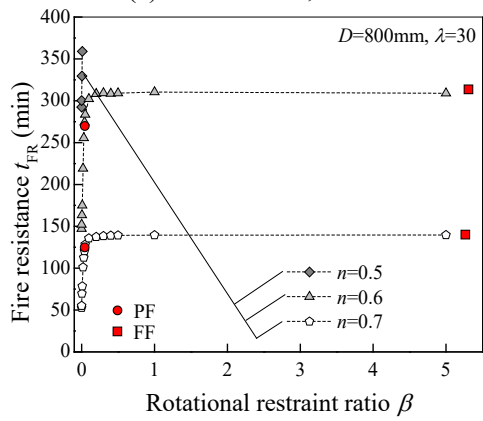
(d)  $D = 400 \text{ mm}, \lambda = 50$



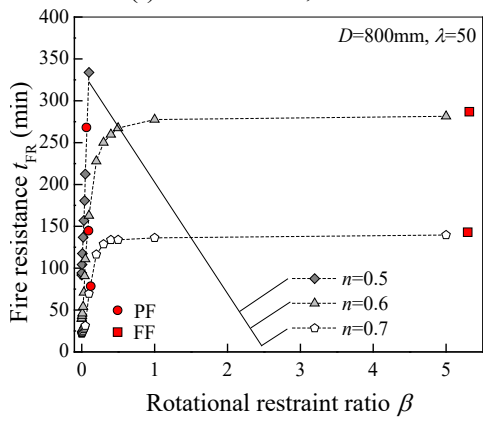
(e)  $D = 600 \text{ mm}, \lambda = 30$



(f)  $D = 600 \text{ mm}, \lambda = 50$



(g)  $D = 800 \text{ mm}, \lambda = 30$



(h)  $D = 800 \text{ mm}, \lambda = 50$

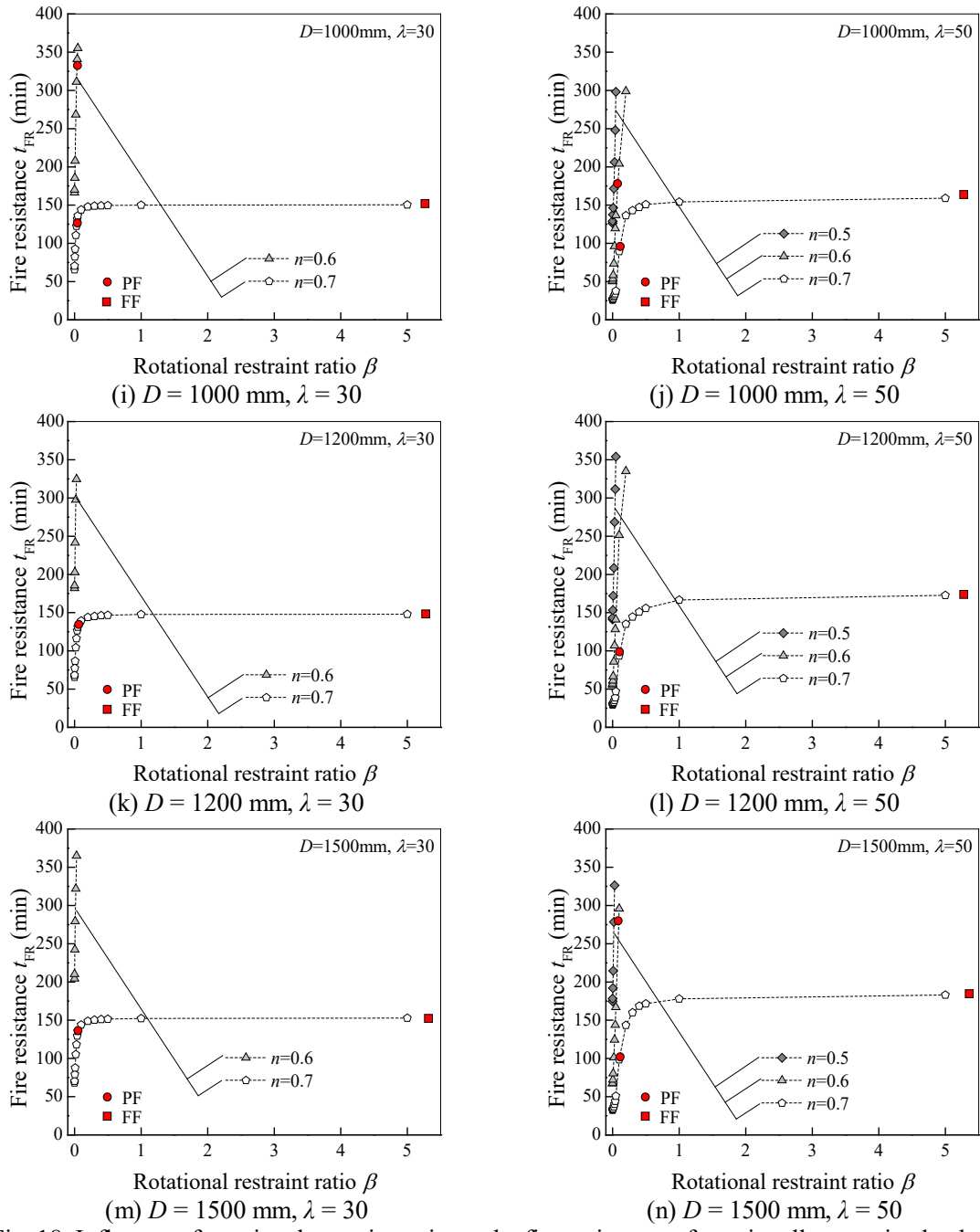
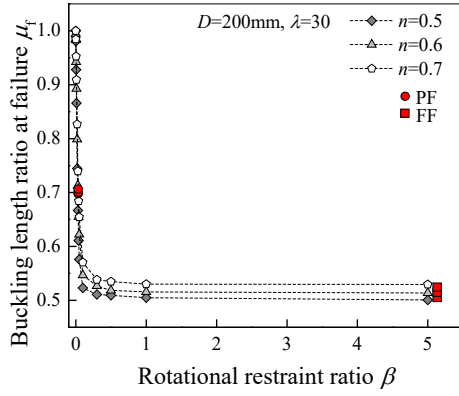
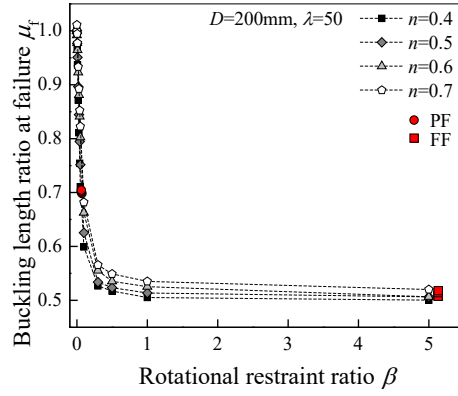


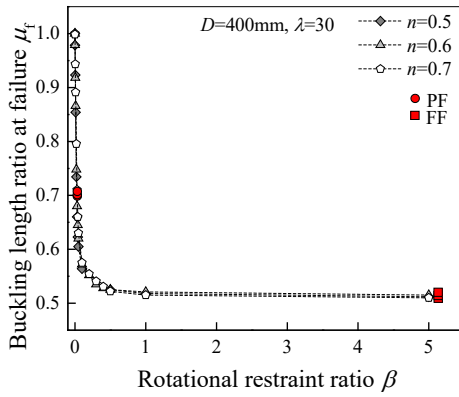
Fig. 18. Influence of rotational restraint ratio on the fire resistance of rotationally-restrained columns



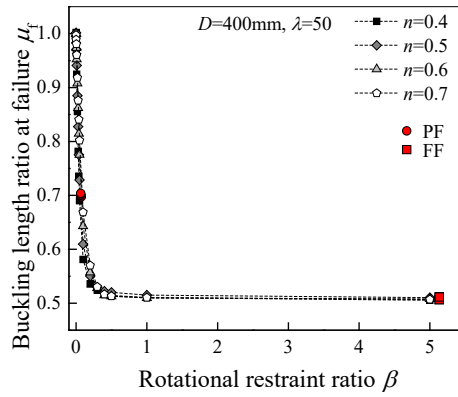
(a)  $D = 200 \text{ mm}$ ,  $\lambda = 30$



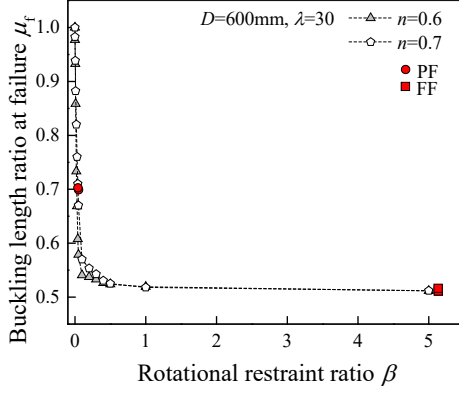
(b)  $D = 200 \text{ mm}$ ,  $\lambda = 50$



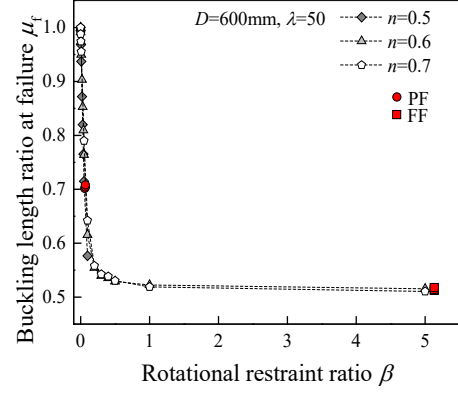
(c)  $D = 400 \text{ mm}$ ,  $\lambda = 30$



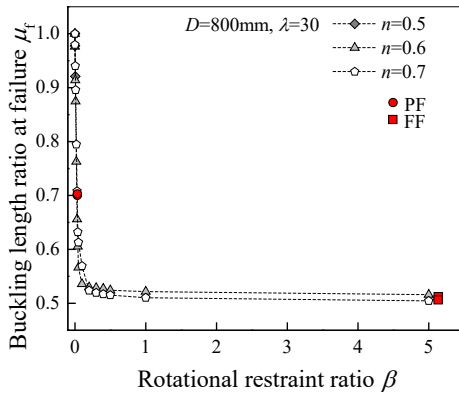
(d)  $D = 400 \text{ mm}$ ,  $\lambda = 50$



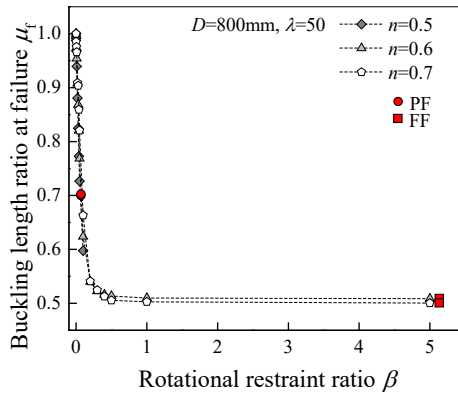
(e)  $D = 600 \text{ mm}$ ,  $\lambda = 30$



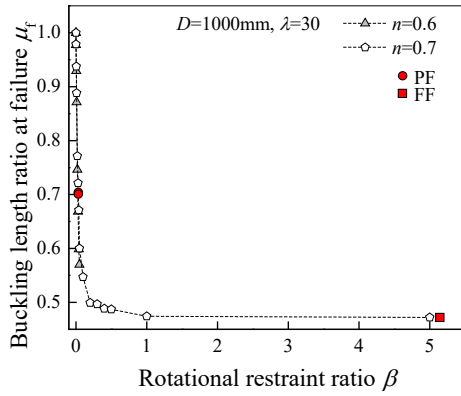
(f)  $D = 600 \text{ mm}$ ,  $\lambda = 50$



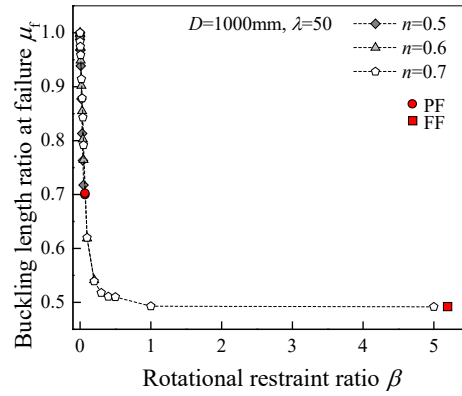
(g)  $D = 800 \text{ mm}$ ,  $\lambda = 30$



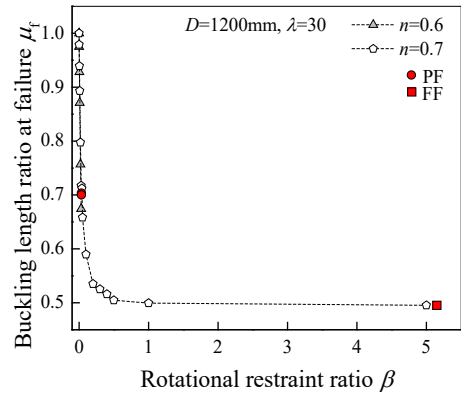
(h)  $D = 800 \text{ mm}$ ,  $\lambda = 50$



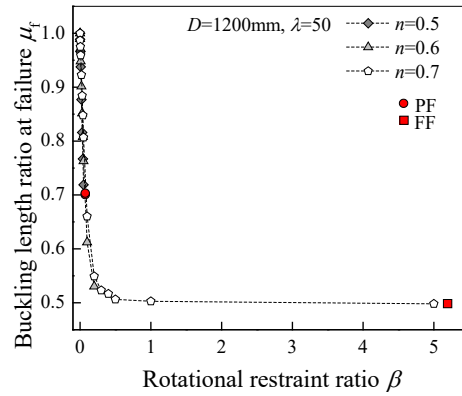
(i)  $D = 1000 \text{ mm}$ ,  $\lambda = 30$



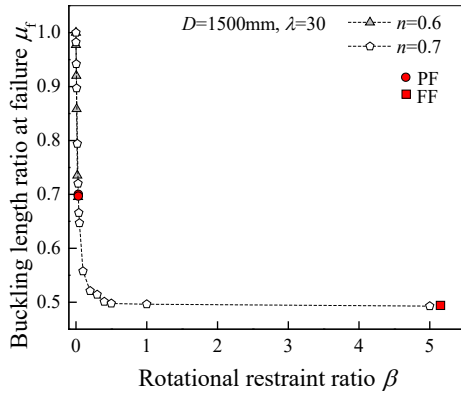
(j)  $D = 1000 \text{ mm}$ ,  $\lambda = 50$



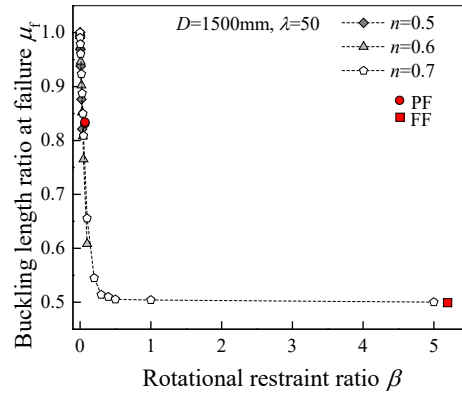
(k)  $D = 1200 \text{ mm}$ ,  $\lambda = 30$



(l)  $D = 1200 \text{ mm}$ ,  $\lambda = 50$

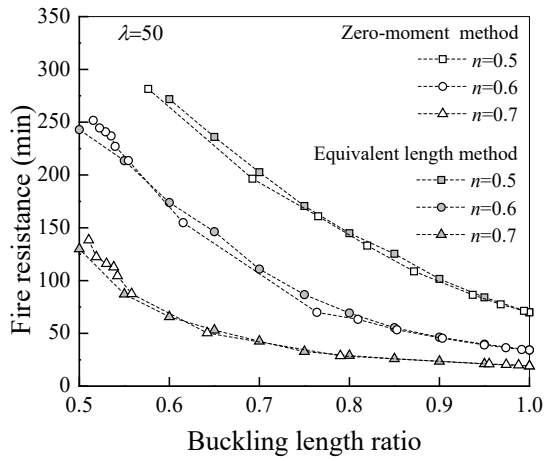
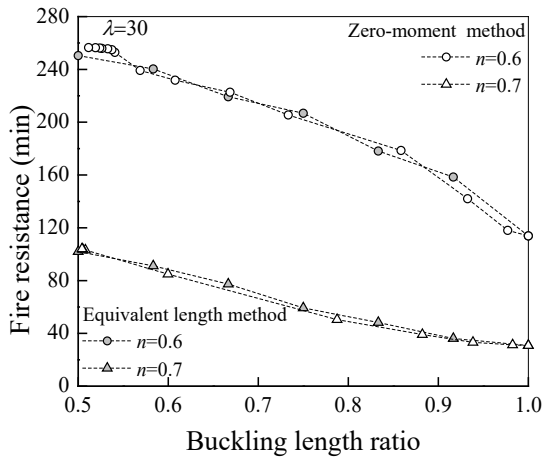


(m)  $D = 1500 \text{ mm}$ ,  $\lambda = 30$

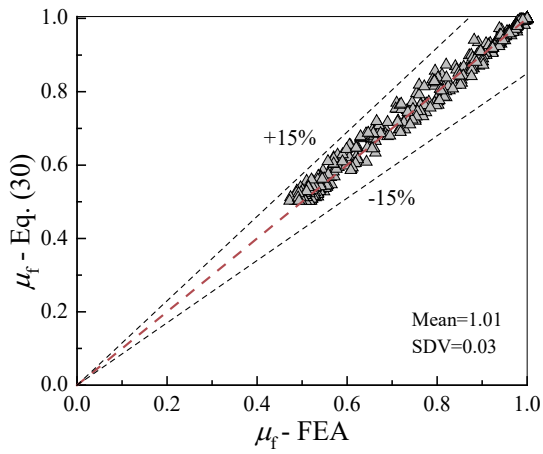


(n)  $D = 1500 \text{ mm}$ ,  $\lambda = 50$

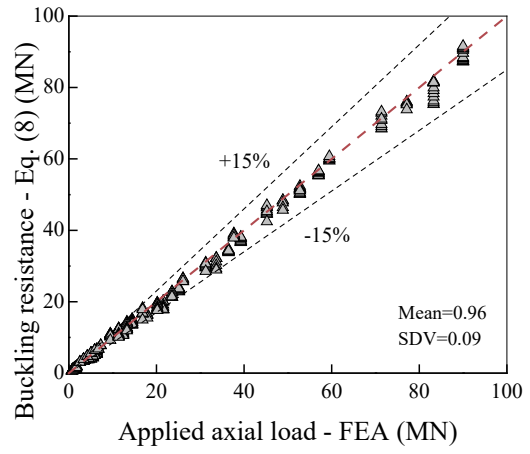
Fig. 19. Influence of rotational restraint on the buckling length ratio at failure for rotationally restrained columns



(a)  $\lambda = 30$  (b)  $\lambda = 50$   
 Fig. 20. Comparison of buckling length ratios calculated by zero-moment and equivalent length methods (cross-section size,  $D = 600$  mm)

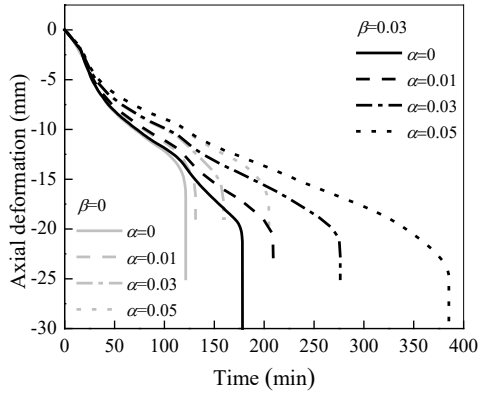


(a) Buckling length ratio at failure

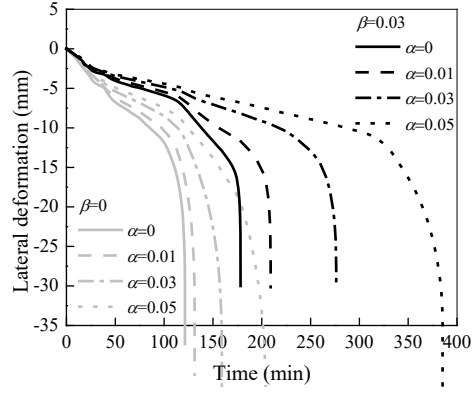


(b) Buckling resistance

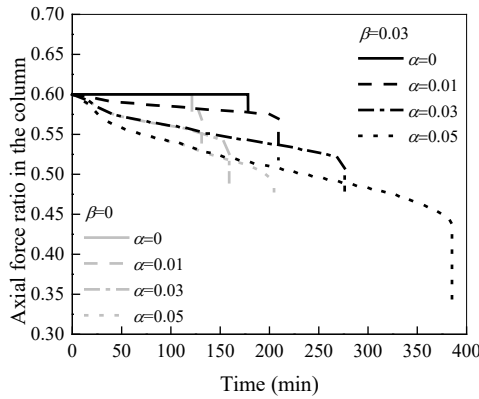
Fig. 21. Predictions for the buckling length ratio at failure and buckling resistance by the proposed method



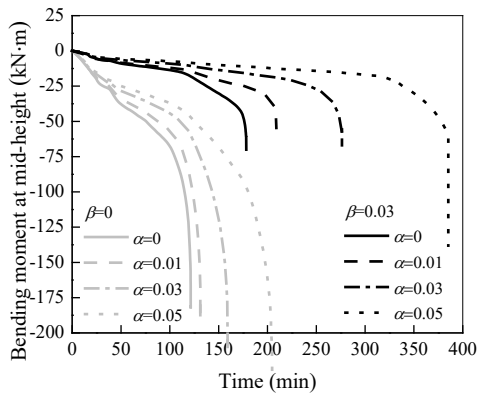
(a) Axial deformation



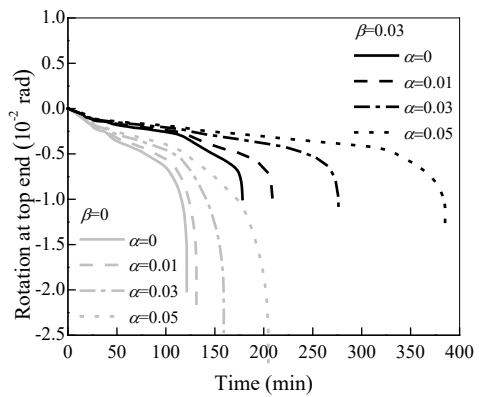
(b) Lateral deformation



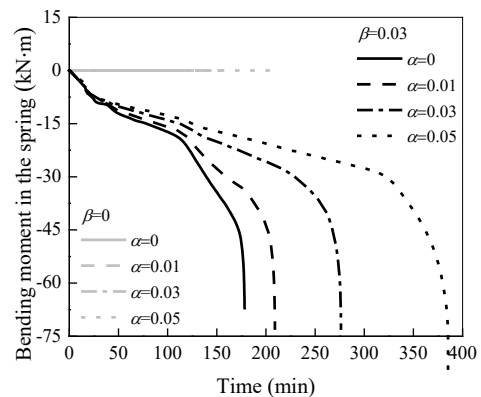
(c) Axial force ratio in the column



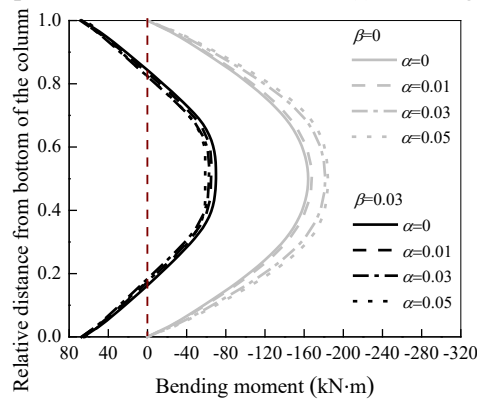
(d) Bending moment at mid-height



(e) Rotation at top end



(f) Bending moment in the spring



(g) Distribution of bending moments

Fig. 22. Influence of axial restraint ratio on the fire behaviour of columns with combined axial and rotational restraints ( $D = 600$  mm,  $\lambda = 30$ ,  $n = 0.6$ )

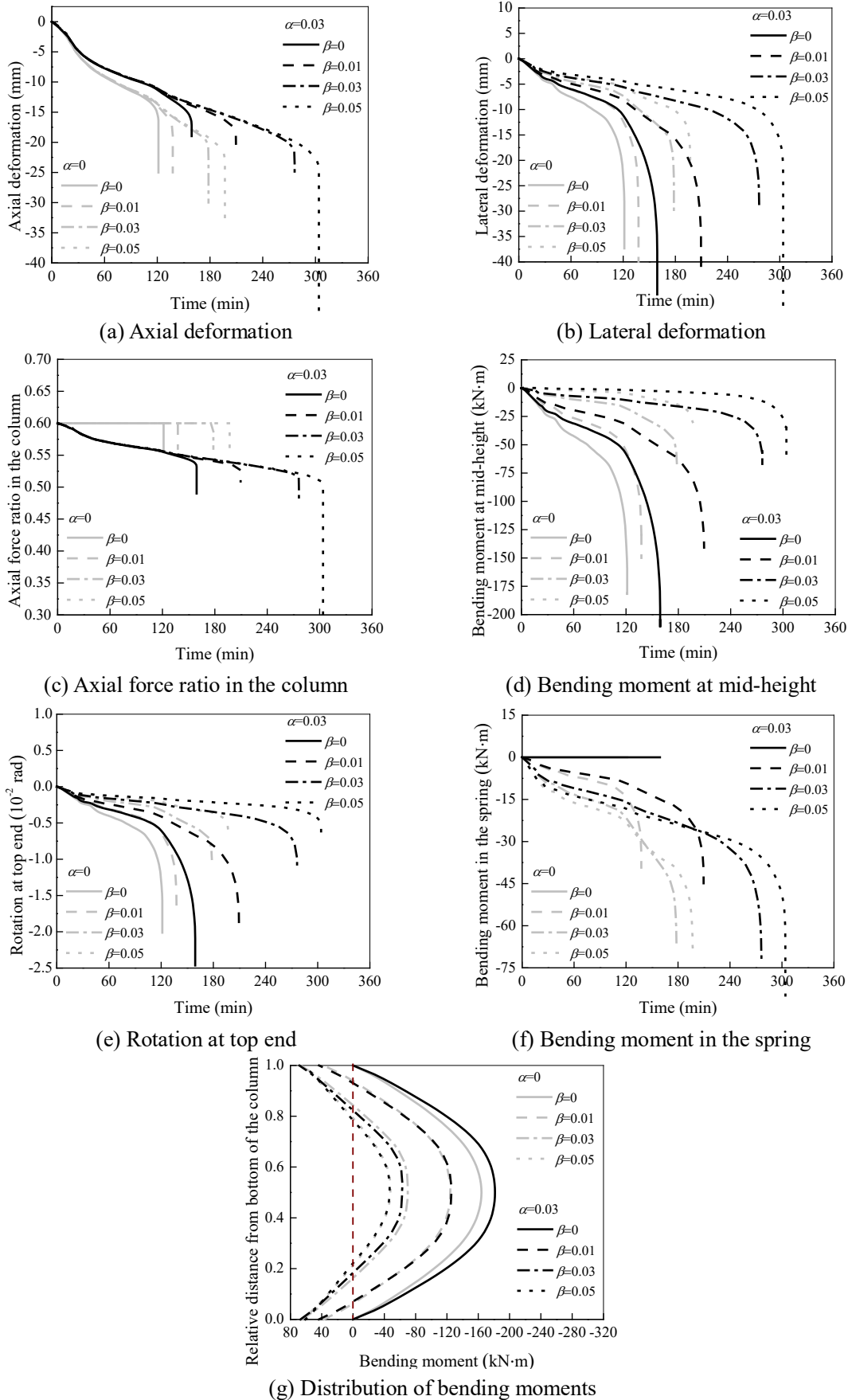
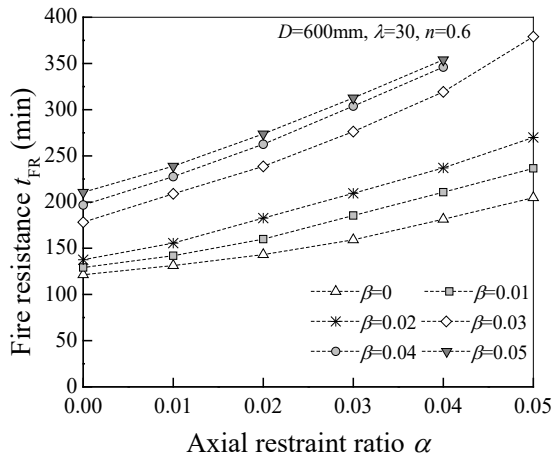
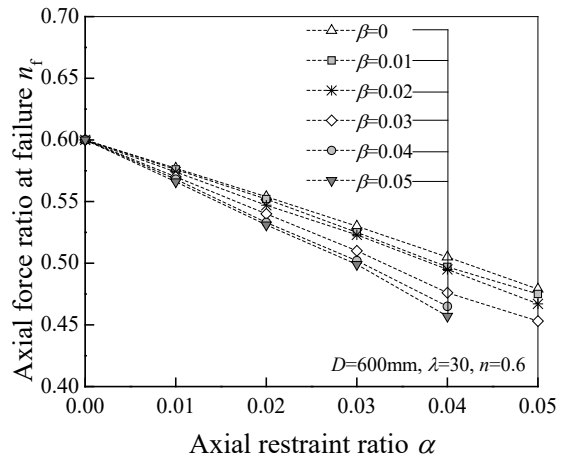


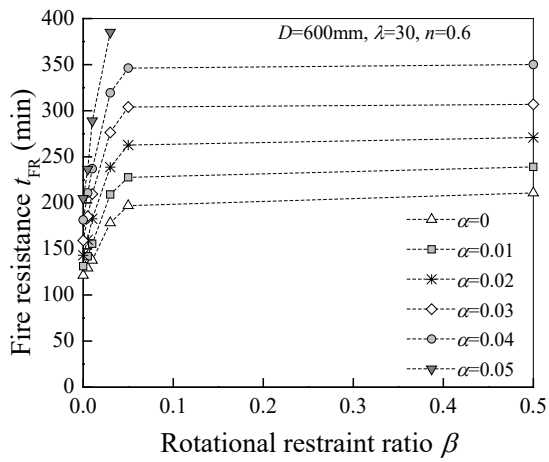
Fig. 23. Influence of rotational restraint ratio on the fire behaviour of columns with combined axial and rotational restraints ( $D = 600$  mm,  $\lambda = 30$ ,  $n = 0.6$ )



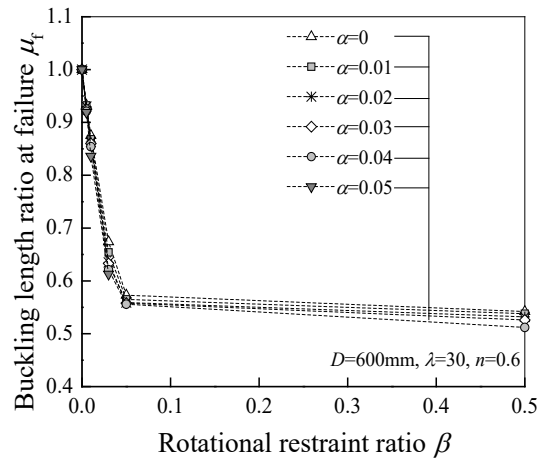
(a) Fire resistance vs axial restraint ratio



(b) Axial force ratio at failure vs axial restraint ratio



(c) Fire resistance vs rotational restraint ratio



(d) Buckling length ratio at failure vs rotational restraint ratio

Fig. 24. Influence of axial and rotational restraint ratios on the fire resistance, axial force ratio and buckling length ratio at failure for the columns with  $D = 600\text{ mm}$ ,  $\lambda = 30$ ,  $n = 0.6$

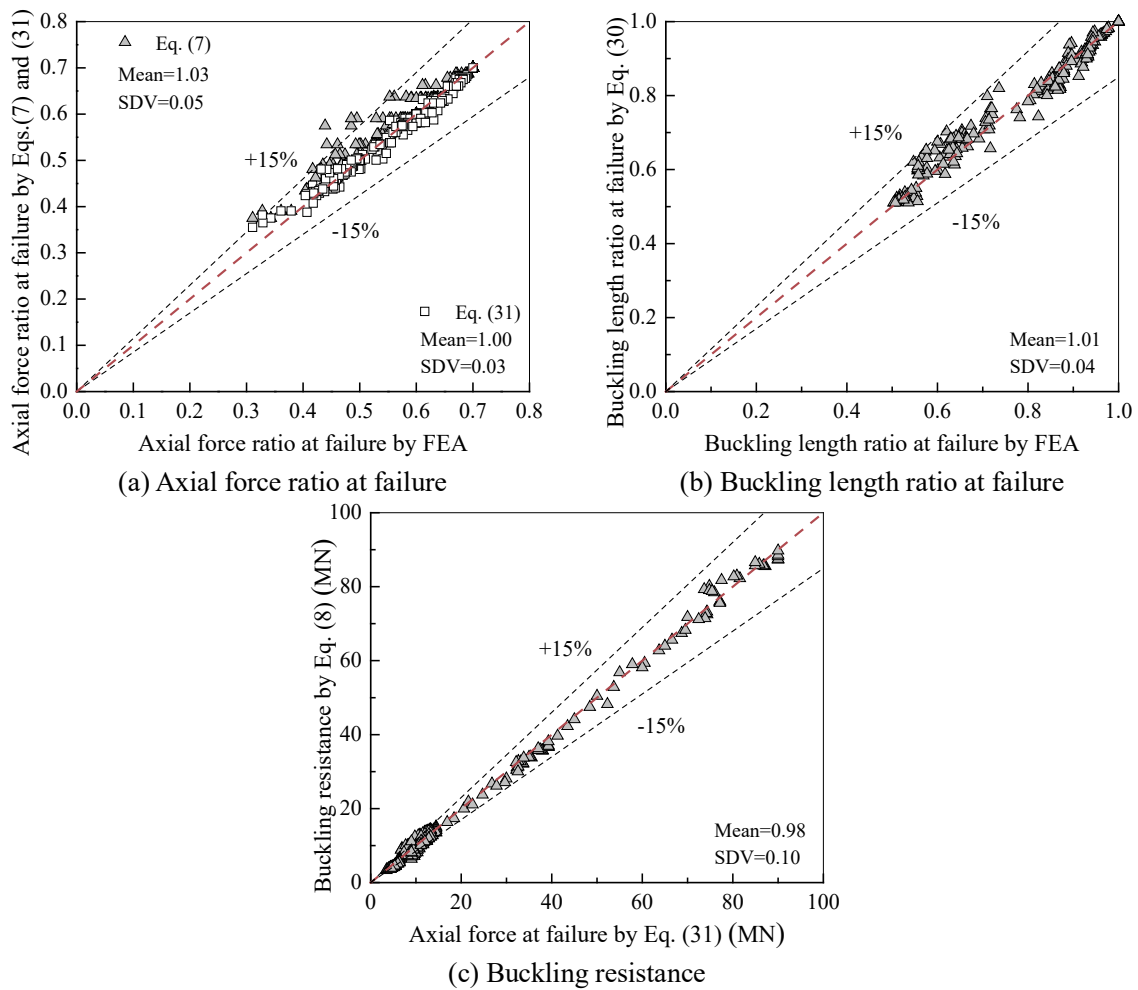


Fig. 25. Comparison of the axial force ratio and buckling length ratio at failure and the buckling resistance between the predicted values and FEA results

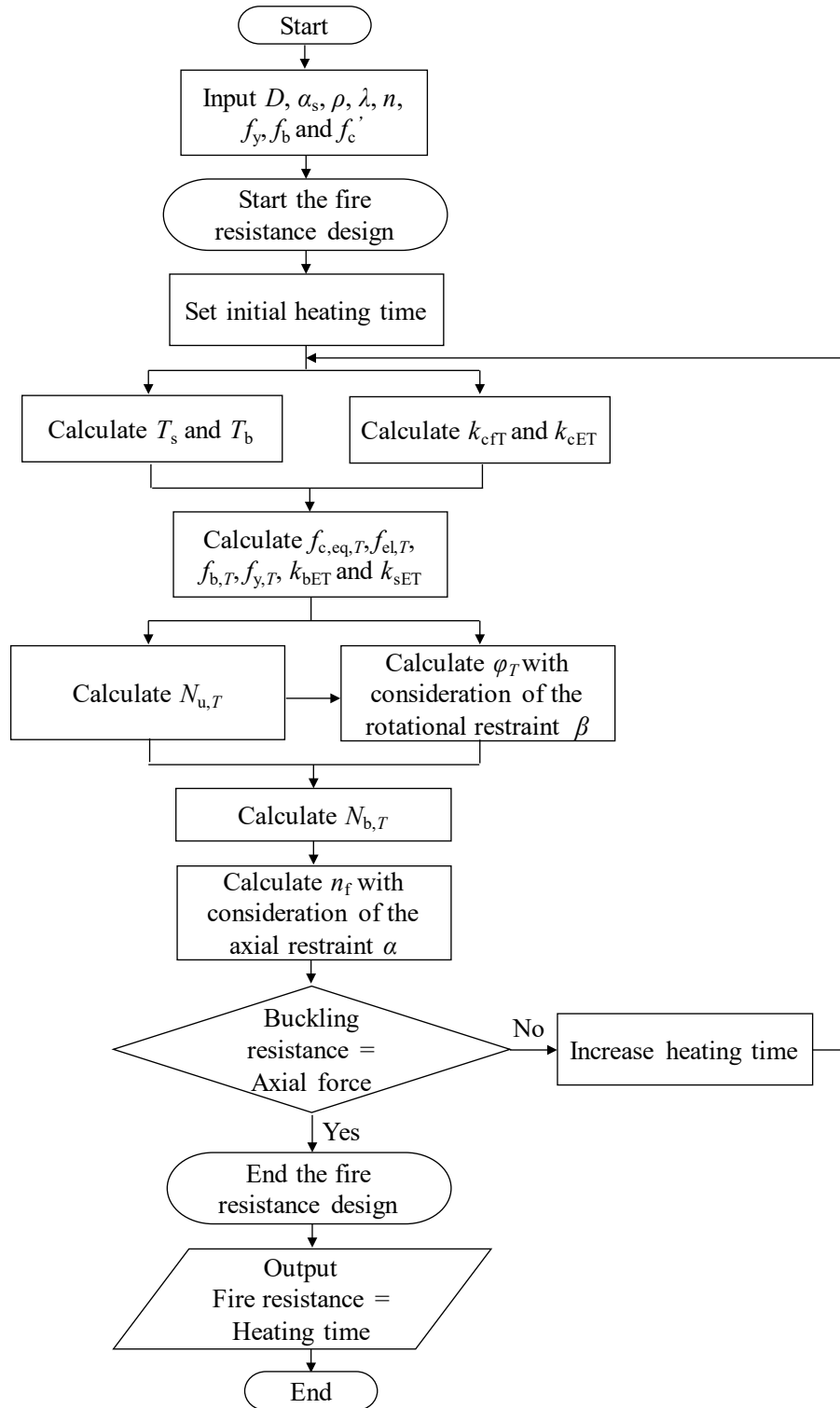


Fig. 26. Flow chart for the fire resistance design procedure of square TRC columns with axial and rotational end restraints

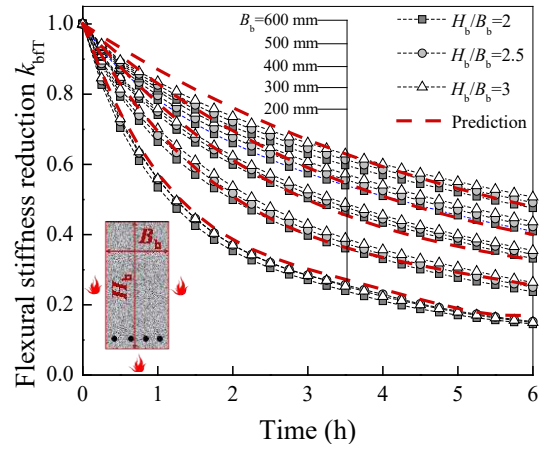


Fig. 27. Reduction of flexural stiffness in the rectangular RC beams heated on three sides

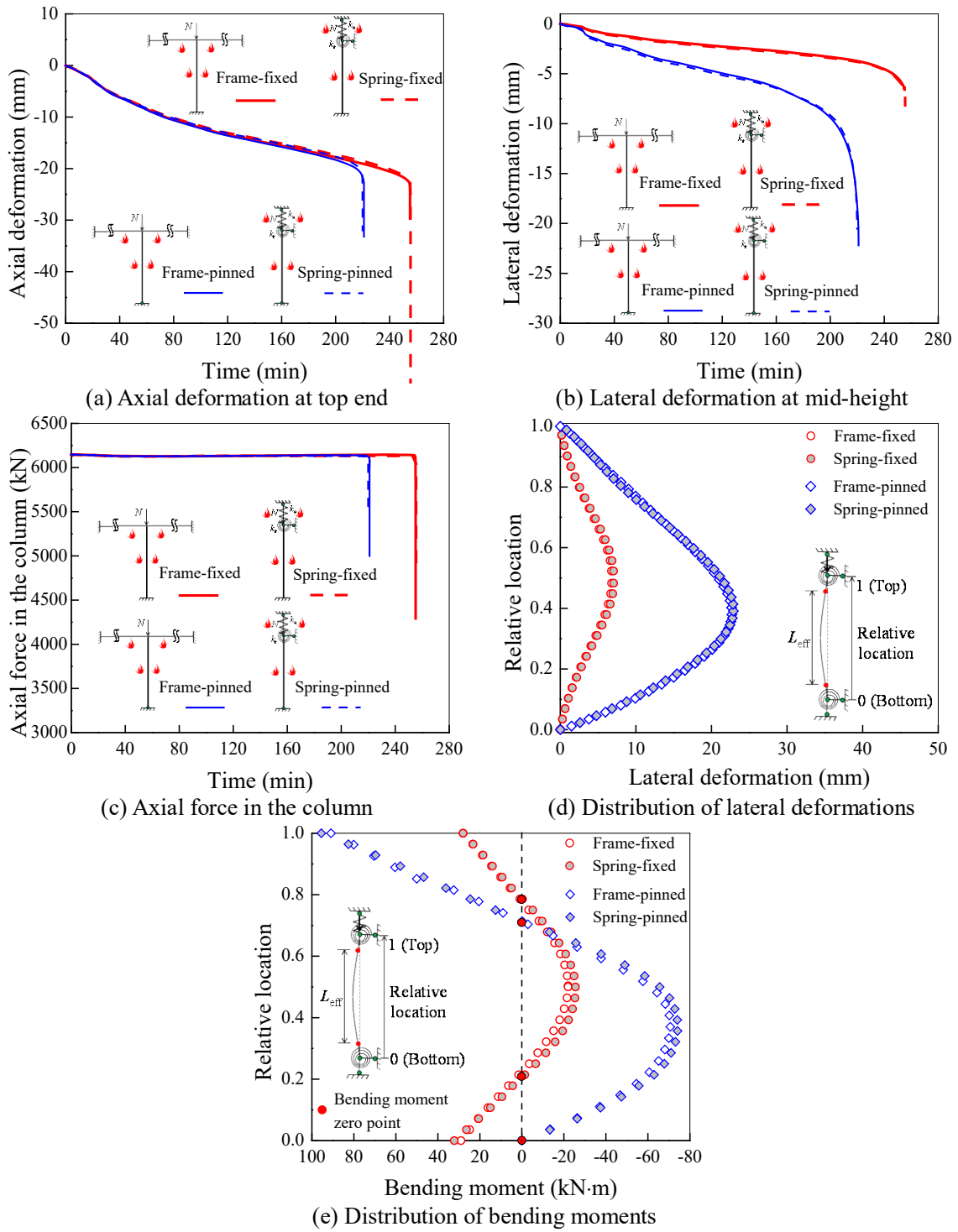


Fig. 28. Validation of the spring model against the frame modelling with heated beams

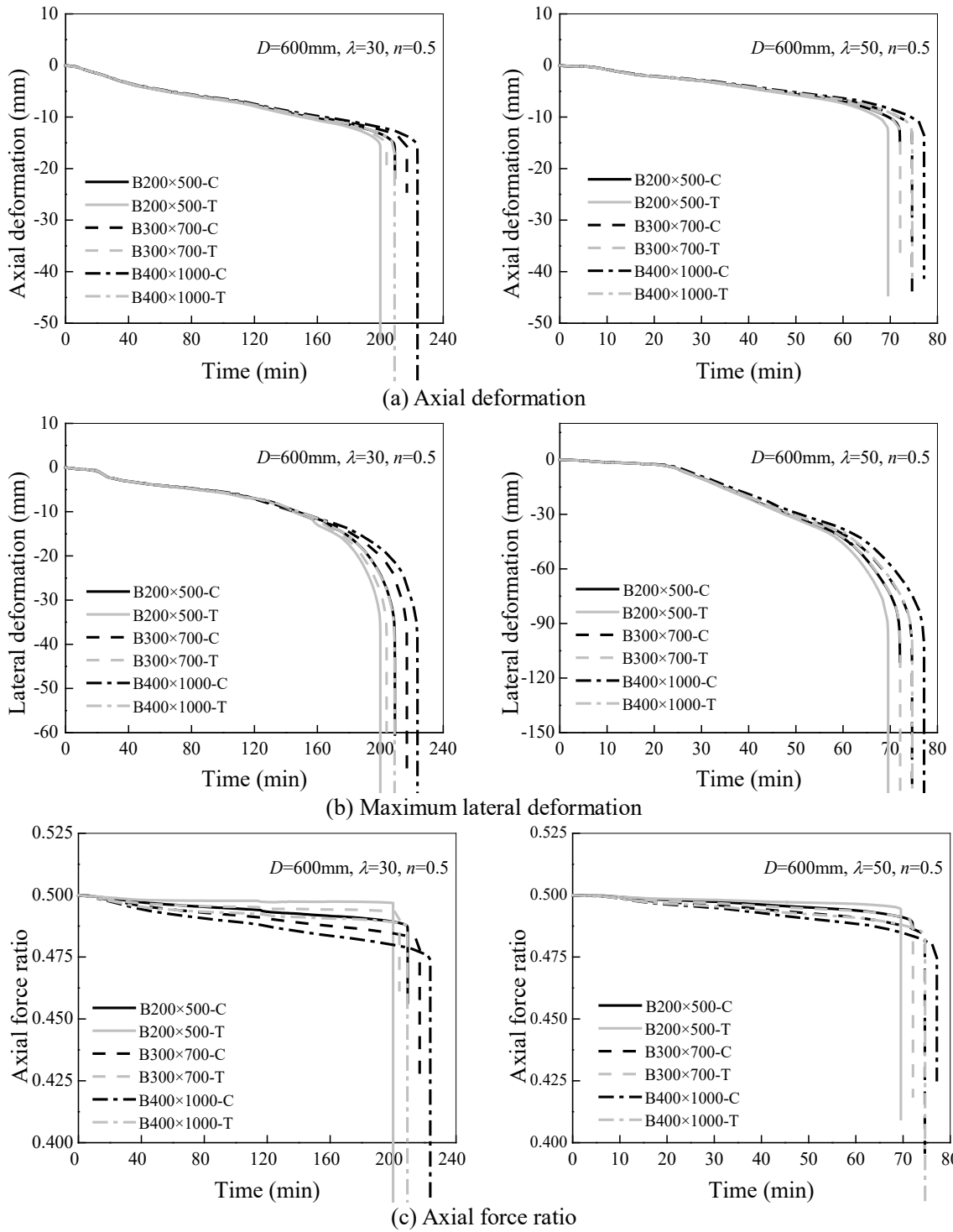
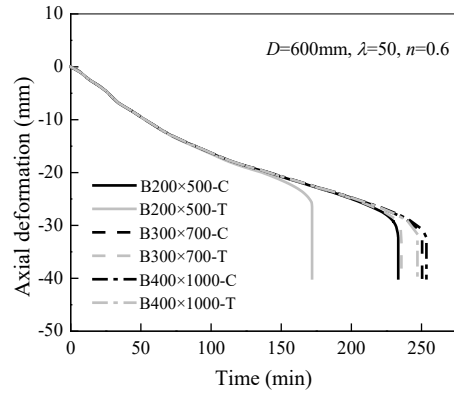
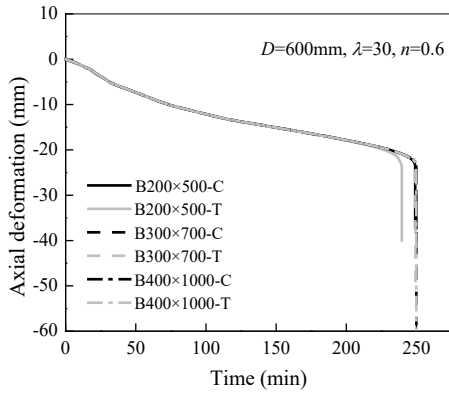
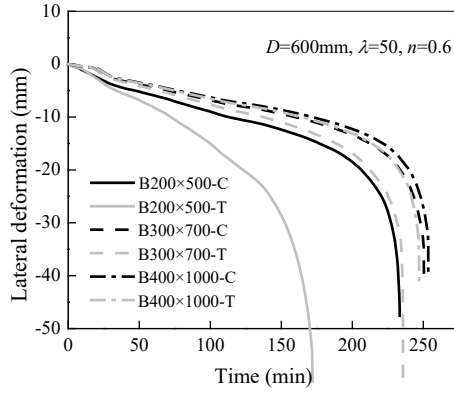
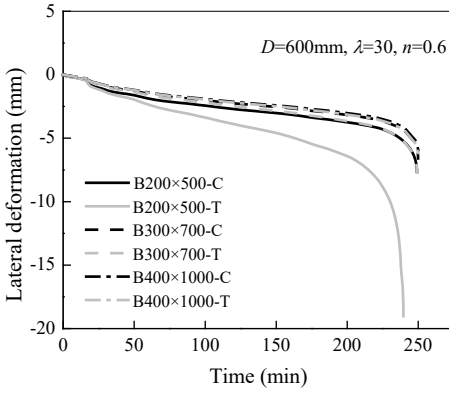


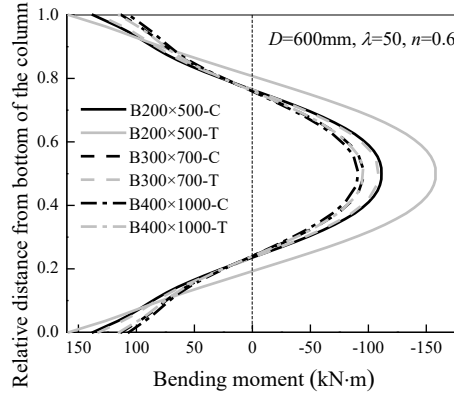
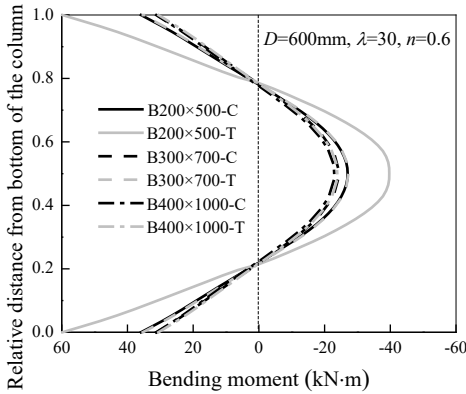
Fig. 29. Influence of temperature-dependent axial restraint on fire performance ( $D = 600 \text{ mm}$ ,  $n = 0.5$ )



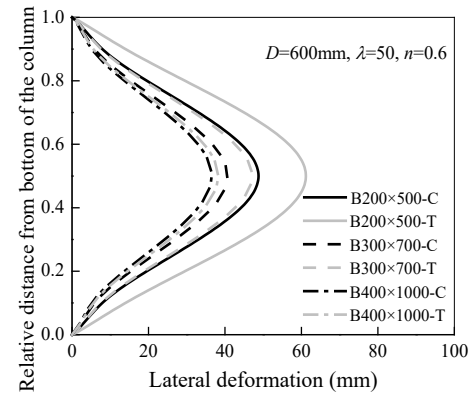
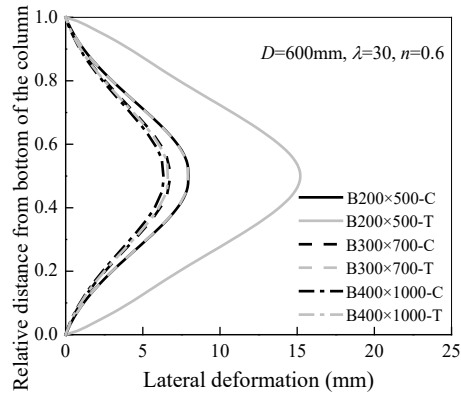
(a) Axial deformation



(b) Maximum lateral deformation



(c) Distribution of bending moments



(d) Distribution of lateral deformations

Fig. 30. Influence of temperature-dependent rotational restraint on fire performance ( $D = 600 \text{ mm}$ ,  $n = 0.6$ )

## Tables

Table 1

Details of the collected fire tests on end-restrained CFST columns

CFST columns	Section	$D \times t_s$ or $H \times B \times t_s$ (mm)	$L$ ( $L_e$ ) (m)	Rebars	$f_y$ (MPa)	$f_c'$ (MPa)	$f_b$ (MPa)	$k_a$ (kN/mm)	$k_{r1}$ & $k_{r2}$ (kN·m/rad)	$P_0$ (kN)	$t_{cr}$ (min)		$P_{max}/P_0$		
											Test	FEA	Test	FEA	
Ref. [28]	A01	Circular	168.3×6	3 (2.5)	-	430.5	28 <sup>x</sup>	-	13	4091 & 1992	816	16	17.3	1.11	1.09
	A02	Circular	168.3×6	3 (2.5)	6 $\phi$ 10	430.5	28 <sup>x</sup>	505.7	13	4091 & 1992	874	13	16.1	1.03	1.06
	A06	Circular	219.1×6	3 (2.5)	-	529	28 <sup>x</sup>	-	13	4091 & 1992	1359	16	17.6	1.05	1.05
	A07	Circular	219.1×6	3 (2.5)	6 $\phi$ 12	529	28 <sup>x</sup>	505.7	13	4091 & 1992	1478	19	18.6	1.06	1.03
	A11	Circular	168.3×6	3 (2.5)	-	430.5	28 <sup>x</sup>	-	13	4091 & 1992	350	27	31.6	1.41	1.49
	A12	Circular	168.3×6	3 (2.5)	6 $\phi$ 10	430.5	28 <sup>x</sup>	505.7	13	4091 & 1992	375	30	32.6	1.39	1.45
	A16	Circular	219.1×6	3 (2.5)	-	529	28 <sup>x</sup>	-	13	4091 & 1992	583	27	33.6	1.24	1.31
	A17	Circular	219.1×6	3 (2.5)	6 $\phi$ 12	529	28 <sup>x</sup>	505.7	13	4091 & 1992	633	43	46.1	1.20	1.27
	A21	Circular	168.3×6	3 (2.5)	-	430.5	28 <sup>x</sup>	-	128	5079 & 2536	816	15	16.6	1.14	1.23
	A22	Circular	168.3×6	3 (2.5)	6 $\phi$ 10	430.5	28 <sup>x</sup>	505.7	128	5079 & 2536	874	17	18.9	1.35	1.28
	A26	Circular	219.1×6	3 (2.5)	-	529	28 <sup>x</sup>	-	128	5079 & 2536	1359	16	16.9	1.11	1.22
	A27	Circular	219.1×6	3 (2.5)	6 $\phi$ 12	529	28 <sup>x</sup>	505.7	128	5079 & 2536	1478	19	18.2	1.12	1.28
	A31	Circular	168.3×6	3 (2.5)	-	430.5	28 <sup>x</sup>	-	128	5079 & 2536	350	26	30.3	1.82	2.21
	A32	Circular	168.3×6	3 (2.5)	6 $\phi$ 10	430.5	28 <sup>x</sup>	505.7	128	5079 & 2536	375	31	35.5	2.08	2.36
	A36	Circular	219.1×6	3 (2.5)	-	529	28 <sup>x</sup>	-	128	5079 & 2536	583	21	25.8	1.66	2.03
	A37	Circular	219.1×6	3 (2.5)	6 $\phi$ 12	529	28 <sup>x</sup>	505.7	128	5079 & 2536	633	46	54.5	1.80	2.08
	Ref. [29]	SC220-30ka	Square	220×10	3.15 (2.5)	4 $\phi$ 16+4 $\phi$ 10	410	33	500*	30	94615 <sup>a</sup>	1125	32.2	38.5	1.34
SC220-110ka		Square	220×10	3.15 (2.5)	4 $\phi$ 16+4 $\phi$ 10	410	33	500*	110	131340 <sup>a</sup>	1125	32.3	37.6	1.75	1.65
SC150-30ka		Square	150×8	3.15 (2.5)	4 $\phi$ 12	410	33	500*	30	94615 <sup>a</sup>	533	24.5	28.2	1.45	1.51
SC150-110ka		Square	150×8	3.15 (2.5)	4 $\phi$ 12	410	33	500*	110	131340 <sup>a</sup>	533	23.4	27.3	1.96	1.82

Table 1 (cont'd) Details of the collected fire tests on end-restrained CFST columns

CFST columns	Section	$D \times t_s$ or $H \times B \times t_s$ (mm)	$L$ ( $L_c$ ) (m)	Rebars	$f_y$ (MPa)	$f'_c$ (MPa)	$f_b$ (MPa)	$k_a$ (kN/mm)	$k_{r1}$ & $k_{r2}$ (kN·m/rad)	$P_0$ (kN)	$t_{cr}$ (min)		$P_{max}/P_0$		
											Test	FEA	Test	FEA	
Ref. [29]	CC273-30ka	Circular	273×10	3.15 (2.5)	4 $\phi$ 16+4 $\phi$ 10	365	33	500*	30	94615 <sup>a</sup>	1144	36.5	40.8	1.25	1.30
	CC273-110ka	Circular	273×10	3.15 (2.5)	4 $\phi$ 16+4 $\phi$ 10	365	33	500*	110	131340 <sup>a</sup>	1144	35.6	41.8	1.67	1.64
	CC194-30ka	Circular	193.7×8	3.15 (2.5)	4 $\phi$ 12	365	33	500*	30	94615 <sup>a</sup>	587	34.7	39.3	1.43	1.52
	CC194-110ka	Circular	193.7×8	3.15 (2.5)	4 $\phi$ 12	365	33	500*	110	131340 <sup>a</sup>	587	31.3	35.5	1.76	1.93
	RC350-30ka	Rectangular	350×150×10	3.15 (2.5)	4 $\phi$ 16+2 $\phi$ 10	420	33	500*	30	94615 <sup>a</sup>	1164	28.4	34.5	1.12	1.32
	RC350-110ka	Rectangular	350×150×10	3.15 (2.5)	4 $\phi$ 16+2 $\phi$ 10	420	33	500*	110	131340 <sup>a</sup>	1164	32	35.7	1.75	1.85
	RC250-30ka	Rectangular	250×150×10	3.15 (2.5)	4 $\phi$ 16	420	33	500*	30	94615 <sup>a</sup>	905	32.5	40.3	1.35	1.43
	RC250-110ka	Rectangular	250×150×10	3.15 (2.5)	4 $\phi$ 16	420	33	500*	110	131340 <sup>a</sup>	905	29.5	36.3	1.96	1.97
Ref. [30]	SC220-30ka-PP	Square	220×10	3.15 (2.5)	4 $\phi$ 16+4 $\phi$ 10	410	33	500*	30	0	1088	40.2	45.5	1.23	1.31
	SC150-30ka-PP	Square	150×8	3.15 (2.5)	4 $\phi$ 12	410	33	500*	30	0	488	24.4	22.5	1.37	1.41
	CC273-30ka-PP	Circular	273×10	3.15 (2.5)	4 $\phi$ 16+4 $\phi$ 10	365	33	500*	30	0	1128	37.2	38.5	1.16	1.28
	CC194-30ka-PP	Circular	193.7×8	3.15 (2.5)	4 $\phi$ 12	365	33	500*	30	0	571	35.9	22	1.31	1.42
	RC350-30ka-PP	Rectangular	350×150×10	3.15 (2.5)	4 $\phi$ 16+2 $\phi$ 10	420	33	500*	30	0	1080	29.2	24.5	1.23	1.35
	RC250-30ka-PP	Rectangular	250×150×10	3.15 (2.5)	4 $\phi$ 16	420	33	500*	30	0	835	37.7	32.5	1.26	1.39

Notes: “ $D$ ” section size in a square or circular column; “ $H$ ” section depth of a rectangular column; “ $B$ ” section width of a rectangular column; “ $t_s$ ” wall thickness of a steel tube; “ $\phi$ ” diameter of a reinforcing bar; “ $L$ ” total length of the column; “ $L_c$ ” column length exposed to fire; “ $f_y$ ” yield strength of the steel tube; “ $f'_c$ ” cylinder strength of the concrete; “ $f_b$ ” yield strength of the reinforcing bars; “ $k_a$ ” axial restraint stiffness; “ $k_{r1}$ ” rotational restraint stiffness about the first principal axis; “ $k_{r2}$ ” rotational restraint stiffness about the second principal axis; “ $P_0$ ” initial applied load; “ $t_{cr}$ ” critical time; “ $P_{max}$ ” maximum axial compressive force inside the column; “ $\times$ ” average cylinder strength of the concrete calculated on account of the cube strengths at the ages of the first test (34.2 MPa) and the last test (35.8 MPa); “\*” nominal yield strength of the reinforcing bars determined by the provided strength grade (B500); “ $\text{ab}$ ” rotational restraints in the two bending directions are equal.

Table 2

Influence of temperature-dependent axial restraint on the fire behaviour of the column ( $D = 600$  mm)

$\lambda$	$n$	Axial restraint	$t_{FR}$	$\alpha_i$	$\alpha_f$	$n_f$
30	0.5	B200×500-C	209.23	0.0061	-	0.487
		B200×500-T	200.00	0.0061	0.0016	0.497
		B300×700-C	216.88	0.0094	-	0.480
		B300×700-T	204.02	0.0094	0.0036	0.492
		B400×1000-C	223.58	0.0127	-	0.472
		B400×1000-T	209.05	0.0127	0.0061	0.487
30	0.7	B200×500-C	41.13	0.0061	-	0.686
		B200×500-T	33.83	0.0061	0.0043	0.692
		B300×700-C	43.63	0.0094	-	0.682
		B300×700-T	41.49	0.0094	0.0071	0.687
		B400×1000-C	47.75	0.0127	-	0.672
		B400×1000-T	44.49	0.0127	0.0101	0.680
50	0.3	B200×500-C	216.96	0.0102	-	0.290
		B200×500-T	213.43	0.0102	0.0025	0.298
		B300×700-C	220.04	0.0156	-	0.283
		B300×700-T	214.80	0.0156	0.0058	0.295
		B400×1000-C	224.15	0.0211	-	0.276
		B400×1000-T	215.83	0.0211	0.0100	0.292
50	0.5	B200×500-C	72.04	0.0102	-	0.488
		B200×500-T	69.55	0.0102	0.0052	0.494
		B300×700-C	74.62	0.0156	-	0.481
		B300×700-T	72.11	0.0156	0.0100	0.488
		B400×1000-C	77.16	0.0211	-	0.475
		B400×1000-T	74.66	0.0211	0.0151	0.482
50	0.7	B200×500-C	20.84	0.0102	-	0.691
		B200×500-T	20.41	0.0102	0.0081	0.692
		B300×700-C	21.42	0.0156	-	0.688
		B300×700-T	20.57	0.0156	0.0134	0.689
		B400×1000-C	21.89	0.0211	-	0.680
		B400×1000-T	21.14	0.0211	0.0187	0.681

Table 3

Influence of temperature-dependent rotational restraint on the fire behaviour of the column ( $D = 600$  mm)

$\lambda$	$n$	Rotational restraint	$t_{FR}$	$\beta_i$	$\beta_f$	$\mu_f$
30	0.6	B200×500-C	249.09	0.223	-	0.565
		B200×500-T	239.58	0.223	0.051	0.571
		B300×700-C	249.89	0.669	-	0.560
		B300×700-T	249.26	0.669	0.226	0.562
		B400×1000-C	250.09	1.843	-	0.555
		B400×1000-T	249.94	1.843	0.809	0.557
30	0.7	B200×500-C	101.66	0.223	-	0.556
		B200×500-T	95.44	0.223	0.096	0.563
		B300×700-C	103.57	0.669	-	0.523
		B300×700-T	102.99	0.669	0.373	0.525
		B400×1000-C	103.98	1.843	-	0.517
		B400×1000-T	103.85	1.843	1.191	0.517
50	0.5	B200×500-C	356.84	0.372	-	0.531
		B200×500-T	263.06	0.372	0.080	0.637
50	0.6	B200×500-C	233.40	0.372	-	0.529
		B200×500-T	171.99	0.372	0.110	0.615
		B300×700-C	250.42	1.115	-	0.520
		B300×700-T	235.64	1.115	0.388	0.530
		B400×1000-C	253.48	3.071	-	0.519
		B400×1000-T	247.09	3.071	1.355	0.521
50	0.7	B200×500-C	112.91	0.372	-	0.539
		B200×500-T	82.69	0.372	0.175	0.547
		B300×700-C	124.72	1.115	-	0.519
		B300×700-T	116.35	1.115	0.587	0.522
		B400×1000-C	135.33	3.071	-	0.515
		B400×1000-T	125.15	3.071	1.853	0.516